2020

Magnetic Refrigerator Device Based on La (FexCoySi1-x-y)13

Khushar Javed

Theses and Dissertations   Graduate School

2020

Magnetic Refrigerator Device Based on La (FexCoySi1-x-y)13

Khushar Javed

Magnetic Refrigerator Device Based on La (Fe$_x$Co$_y$Si$_{1-x-y}$)$_{13}$

A thesis submitted in partial fulfillment of the requirements for the degree of Master of Science in Mechanical Engineering at Virginia Commonwealth University.

by

Khushar Javed

Master of Science in Mechanical and Nuclear Engineering, Virginia Commonwealth University, 2020

Professor: Dr. Ravi L Hadimani
Department of Mechanical and Nuclear Engineering

Virginia Commonwealth University
Richmond, Virginia
March 2020

Acknowledgment

I would like to thank my husband, Faizan, for his love, support and patience during the past two years it has taken me to graduate. I would like to thank my parents especially my mom for her unending love and support. I would also like to thank Dr. Ravi Hadimani for his help, continuous support and for his direction with this project. Last but not least, I would like to thank Ames Lab for their guidance and providing me the material to use for my thesis.

Table of Contents

Table of Figure

Abstract

By Khushar Javed

Bachelor of Science in Mechanical and Nuclear Engineering

A thesis submitted in partial fulfillment of the requirements for the degree of Master of Science in Engineering at Virginia Commonwealth University.

Virginia Commonwealth University, 2020

Professor: Dr Ravi L Hadimani

Associate professor, Department of Mechanical and Nuclear Engineering

Particles of Lanthanum-iron-silicide, La $(Fe_xCo_ySi_{1-x-y})_{13}$ exhibit different magnetic properties when stored in air compared to the same stored in water. The sample with a nominal composition of La$(Fe_{0.842}Co_{0.073}Si_{0.084})_{13}$ was prepared by arc-melting from elements under argon atmosphere. In recent years, there has been research conducted on different processes that could drastically reduce energy costs of cooling and replacing gas compressors with magnetocaloric materials. Magnetization measurements were carried out on this magnetocaloric material to

characterize it in order to design magnetic refrigerator device based on it. The main focus of this research is to determine and compare magnetic properties of the material when kept in water and air. The samples are divided into four types; milled and non-milled sample kept in air and water. The present work is focused on determining the magnetization of these materials as a function of magnetic field and temperature near Curie temperature, direct measurement of heat capacity, change in entropy, change in temperature and other physical properties. Firstly, we started by comparing results of four samples to analyze them and predict the effect of water on the material. Then, we investigated the change in magnetocaloric effect of non-milled sample stored in water. This research-based analysis was used to design the magnetocaloric heat exchange device US Patent Application No. 16/394,688.

CHAPTER 1

INTRODUCTION

1. INTRODUCTION

1.1. World energy consumption

The energy consumption in the world is increasing every day. With the passage of time, we are going to the age of Energy trilemma (trade-off between decarbonization, energy security and affordability) [1]. We need to manage the energy sources in such a way to ensure energy security and its equity. We not only have to provide clean and environmentally friendly energy but also at an affordable price.

Energy consumption in the residential sector is about 45% of total energy usage [2]. In addition, by the end of 2050, it will be 70% of total world energy usage out of which cooling takes 15% in its different forms from chilling to refrigeration [3]. Therefore, if the efficiency of cooling is increased it will reduce the world's energy consumption. By the end of 2050, it will have a significant impact on energy consumption [4]. Any increase in efficiency will have positive economic and environmental effects.

1.2. Refrigeration in past

Ice houses were used before the invention of the refrigerator. In 1820, Oliver Evans explained vapor-compression refrigeration cycle for the first time, then later in the same year, Michael Faraday liquefied ammonia [5]. Soon after Jacob Perkins developed the first refrigeration system [6]. From the 1850s, all kind of cooling is done with the gas compressor system and later on in

1913, domestic refrigerators were invented. General Electrics (GE) made the first of the domestic refrigerators [7]. The refrigerators became more common from the 1930s onwards, using Freon as the refrigerant, which was harmful to the environment and especially to the ozone layer [8]. These chloro-flouro-carbons contribute to the ozone depletion that results in a major environmental problem as it increases the amount of ultraviolent (UV) radiation reaching the earth surface. Back in 1990, instead of Freon, tetra-flouro ethane was used as a refrigerant as it is less dangerous in comparison to Freon, although it posed health and environmental risks of its own [9].

1.3.   Refrigeration

Refrigeration works on the principle of heat transfer from the contraction and expansion of the refrigerant known as the vapor compression cycle as shown in Figure 1.1
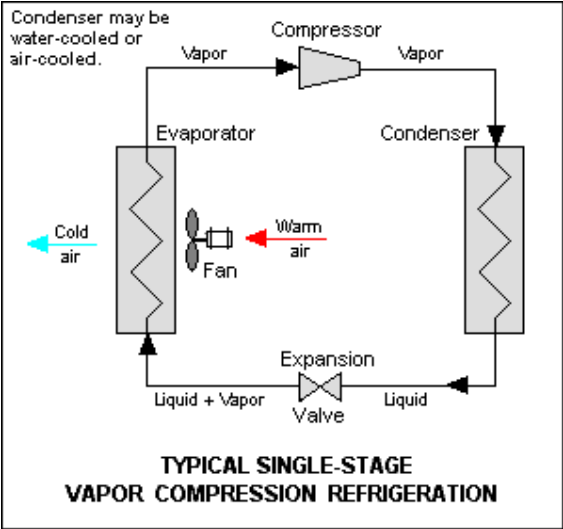
Figure 1.1: Vapor compression cycle [10]

This method has been used for the last 170 years and not much progress has been made on the other refrigeration techniques due to their complex systems, efficiency, durability, and price. The vapor-compression refrigeration cycle consists of four major processes: compression, condensation, expansion and evaporation. During compression process refrigerant is first compressed and as a result it becomes a high-pressure and temperature gas that is passed on to the next step of condensation. During the condensation process the gas is condensed to the liquid state by expelling out the heat. This liquid is then passed through the expansion process where the pressure of liquid is reduced rapidly. Due to the decreased pressure the liquid refrigerant evaporates returning to the gas phase to be recompressed while also absorbing the heat from the surroundings.

However, there is a serious threat to the environment from vapor compression refrigeration as it relies on harmful gases like chlorofluorocarbons (CFCs) and hydrofluorocarbons (HFCs). These compounds have only been utilized for a short time in refrigeration systems, but their emmision is harming the environment vigorously. If these emissions are eliminated, we will help reduce the climate change. The vapor compression cycle has proven to be a durable and cost-effective technology for the past 170 years in spite of its low energy efficiency; its COP is 4. However, we need to find an alternative that can take place of the vapor compression due to its environmental impact.

1.4.   Alternatives

Refrigeration using gas compression and expansion is less expensive, but it has harmful effects on the environment. Due to these environmental concerns, in recent years alternatives to the vapor-compression cycle have been investigated which include

- Thermoacoustic (about 40% efficiency of Carnot) [11]

- Thermoelectric (about 10-15% efficiency of Carnot) [12]

- Magnetic refrigeration (about 60% efficiency of Carnot) [13]

Thermoacoustic refrigeration process works by using the mixture of gases in a resonator and the acoustic waves. Figure 1.3 is a schematic diagram of thermoacoustic device.
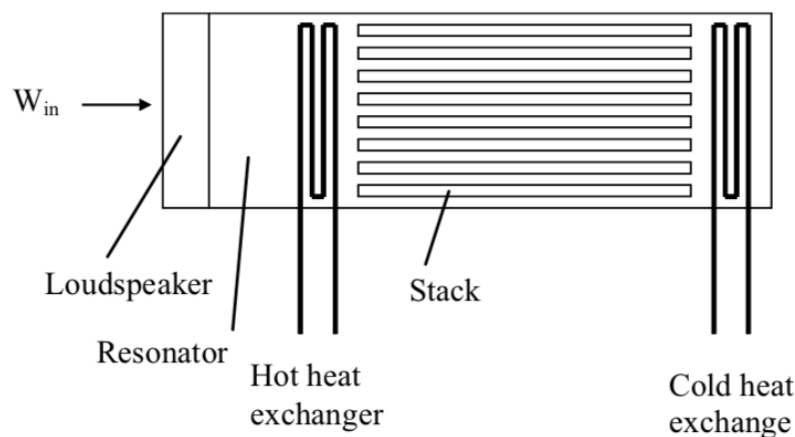
Figure 1.2: Thermoacoustic Engine [14]

Mixture of inert gas is stored in resonator and the acoustic waves are passed into the resonator. The loud acoustic waves result in the resonation of gas in the resonator. The pressure of these sound waves causes the compression and expansion of the gas in the structure annotated as stack

in Figure 1.3. This oscillation of gas creates temperature difference, allowing heat to be expelled out of the cold side of the system.

Thermoelectric cooling operates on the process of Peltier effect principal. According to this principal, a temperature difference is created when heat is transferred between two electrical junctions known as pn-junction. Voltage is applied to the joined conductors that causes the flow of current across them. Due to this flow of current through the joint of these two conductors, temperature difference is created, and heat is expelled out of one conductor as a result cooling occurs while heat is accumulated at the other conductor.

Magnetic refrigeration can be understood as an analogy to the conventional gas expansion and compression system. In magnetic refrigeration, the material is magnetized and then demagnetized to produce the cooling effect. This technology increases the efficiency that is equivalent to 60 percent Carnot efficiency [15]. In addition, this method does not produce any harmful gases in the environment. Noise reduction can be obtained because of less moving parts than a conventional gas system. High pressure is not required so lightweight plastic can be used for this method [16]. The above characteristics make this method an appealing technology for cooling. Additionally, this technology can be used for heating purposes including clothes dryers and water heaters.

CHAPTER 2

MAGNETOCALORIC EFFECT (MCE)

2. MAGNETOCALORIC EFFECT (MCE)

MCE is the cooling and heating of magnetic material with the application of a magnetic field, this is also known as adiabatic demagnetization. The reversible thermal change of a material to a certain field when applied is known as a caloric effect [17]. The caloric effects are distinguished by the nature of the field used. Following are some calorific effects

- Magnetocaloric effect
- Barocaloric effect
- Elastocaloric effect
- Electrocaloric effect

2.1. Principle of magnetocaloric effect

The basic principle of magnetocaloric effect is based on the adiabatic demagnetization. The reversible temperature change of the Magnetocaloric Material (MCM) is achieved when it is exposed to the change in the magnetic field. Figure 2.1 represents the four stages of magnetic refrigeration cycle.
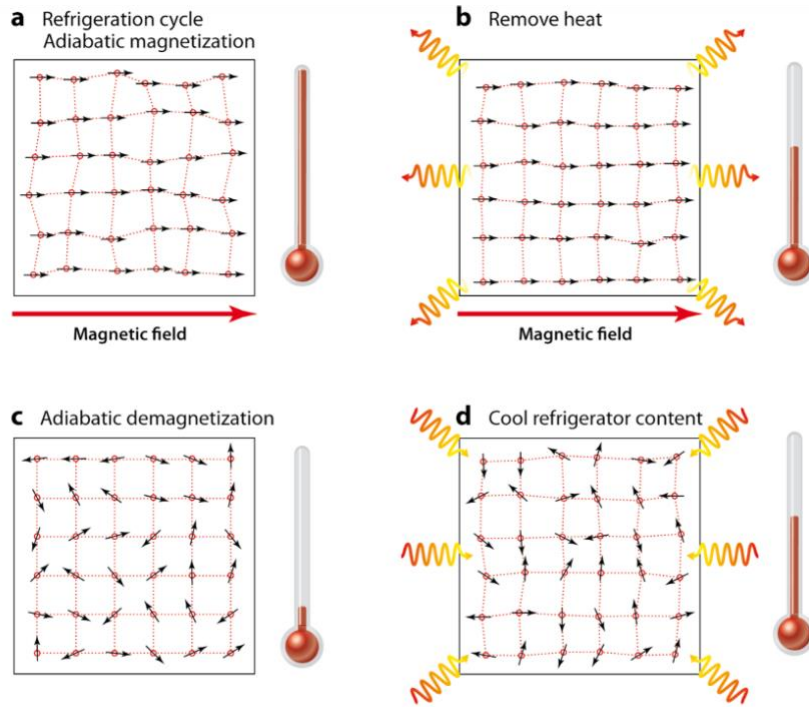
Figure 2.1: The four stages of a magnetic refrigeration cycle:
(a) adiabatic magnetization, (b) remove heat,
(c) adiabatic demagnetization, and (d) cool refrigerator contents [18]

This change in magnetic field affects the spin system of the material that causes the change in the order of the magnetic moments of MCM. Magnetocaloric materials have two types of entropy; lattice entropy and magnetic entropy. When magnetic field is applied the magnetic entropy of the material changes. When a magnetic field is applied under isothermal conditions (temperature is kept constant) the magnetic moment of material is aligned, resulting in a decrease of magnetic entropy. When magnetic field is applied under adiabatic conditions (total entropy is kept constant) the lattice entropy increases to compensate the reduction of the magnetic entropy. This increase in lattice entropy increases the temperature of the material. Based on experimentation, for the paramagnetic materials this prominent increase in lattice entropy and reduction of

magnetic entropy occur near absolute zero whereas for ferromagnetic materials it occurs near the curie temperature.

2.2.   History of magnetocaloric effect

It was named as a "novel magnetocaloric phenomenon" when two scientists P. Weiss and A. Piccard discovered the reversible heating of nickel at 627K (Curie temperature) in 1917 and 1918 [7]. In 1933 MacDougall was first to show the MCE of $Gd_2(SO4)_2 \cdot 8H_2O$ (a paramagnetic salt) that attained a temperature of 0.25K [19], [20]. It then became a laboratory technique to reach very low temperatures (in milliKelvins).

MCE was developed to near room temperature via ferromagnetic material in the late 1970s. Gadolinium was used as a working material for the MCE and a scientist Brown reported that after 50 cycles the minimum temperature attained was 47K utilizing this phenomena Active Magnetic Refrigerator (AMR) was developed [21] providing an alternative to conventional gas compression systems. The AMR cycle steps are shown in the Figure 2.2
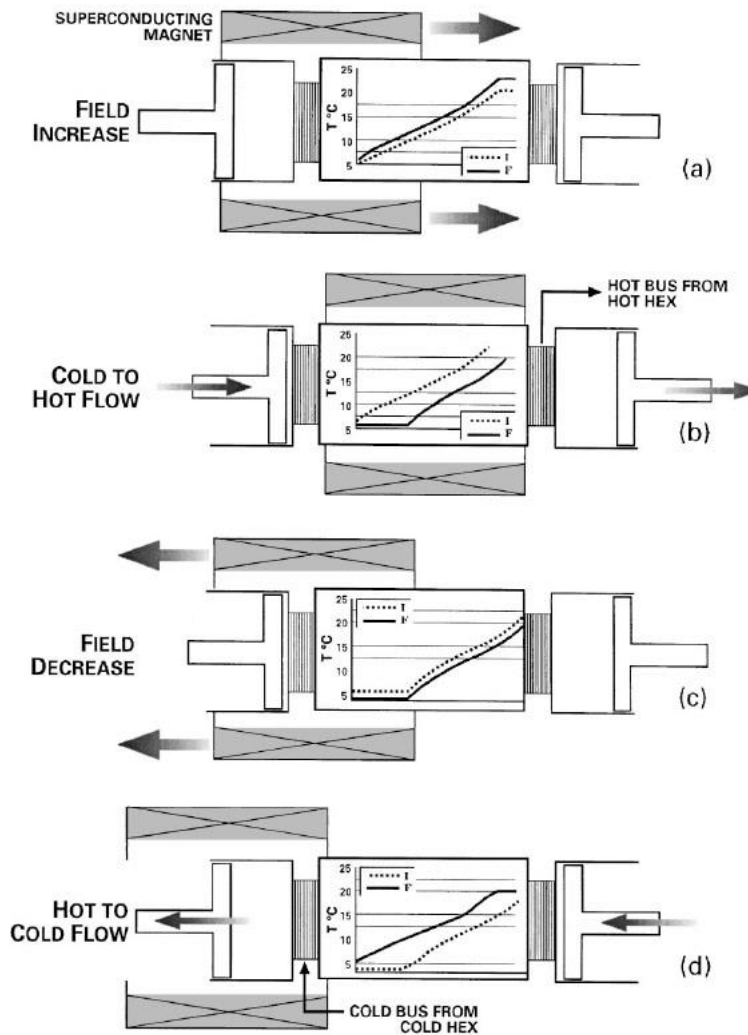
Figure 2.2: AMR cycle steps [22]

This phenomenon allows the system to get the energy at one point in the system and then release it at any other point in the system. The main steps are shown in Figure 2.2. The overall temperature difference can be calculated by the temperature difference between the hot and cold sources. Following are the steps of the AMR cycle

a) Adiabatic magnetization

In a thermally insulated system, when external magnetic field is applied to the magnetocaloric material the temperature of the material is increased.

b) Isofield cooling

This increase in temperature is expelled out to the surroundings by heat exchange medium. During isofield cooling magnetic field is kept constant to prohibit the change in magnetic spin of the system.

c) Adiabatic demagnetization

Once heat is expelled out during isofield cooling the magnetic field is removed keeping the change in total entropy constant. The temperature of magnetocaloric material reduces as a result of its magnetocaloric effect.

d) Isofield heating

During isofield heating the magnetic field is kept constant to avoid the increase in temperature of the magnetocaloric material that is in contact with the heat load. Once the magnetocaloric material and the heat load reaches same temperature, the cooling cycles finishes, and the new cycle begins.

The efficiency of this cycle is determined by the shape and geometry of the regenerator. Working temperature can be extended by using various magnetocaloric material layers. The temperature range can be from 269-293K.

2.3. Development of Magnetocaloric Devices

Gd$_5$Si$_2$Ge$_2$ was demonstrated as a magnetocaloric material and it set up a milestone in the MCE application in 1997 by Gschnieder, et. Al, it was also termed as first-order magneto-structural transformation [9]. 1n 1998, a demonstration unit was developed, and it ran for over 5000 hours with almost no maintenance [9]. The figure shows this unit
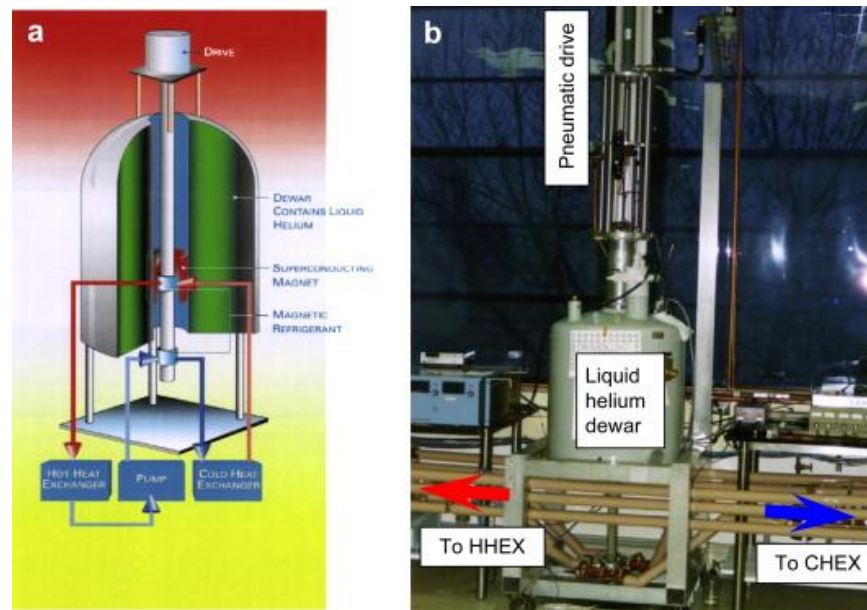
Figure 2.3: MCE demonstration unit [9]

The above simulation was the base of the research in both design and well as in material departments [23]. Haier, BASF, and ACA described the wine cooler concept using the magnetocaloric effect [24]. Then the prototypes were developed on this idea by the BASF [25]. The Figure 2.4 shows the design of wine cooler and 2.5 shows the prototype of the magnetocaloric heat pump.
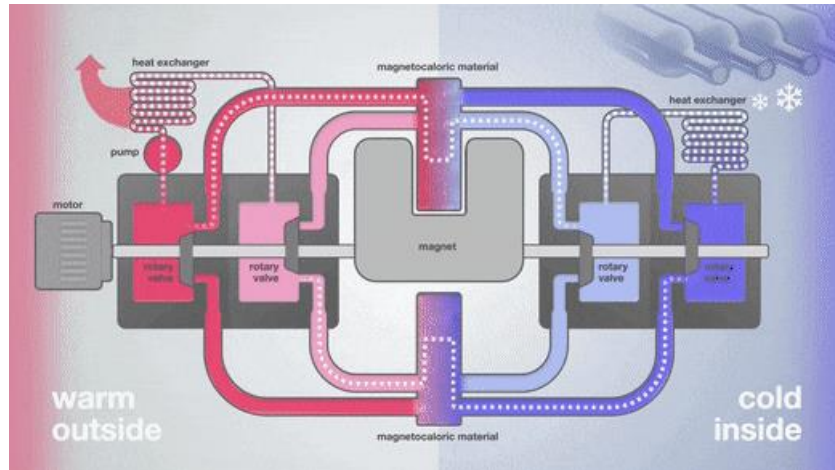
*Figure 2.4: Schematic of working principle of
a magnetocaloric Wine Cooler* [26]
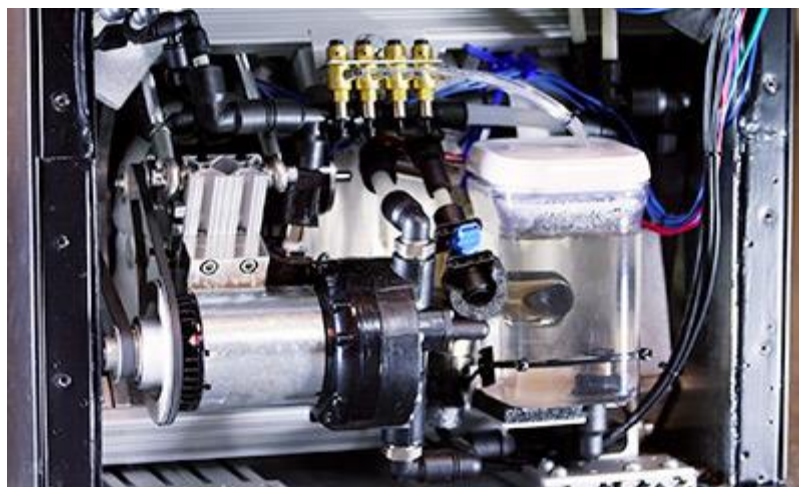
*Figure 2.5: Magnetocaloric Heat Pump Prototype featured
at the CES show in Las Vegas* [27]

The first Magnetic refrigerator was launched in 2016 by a French company Cooltech, offering

200W to 700W refrigerators [28]. These refrigerators are using water as a refrigerant. These

refrigeration systems are used as storage keepers, wine coolers, domestic use, household use and

20KW refrigerators are in progress for industrial cooling which will be available in the future. According to R&M Global Forecast to 2023, the magnetic refrigeration will be at USD 163.7 million by the end of 2023 and it will be growing at a rapid rate of 108% in the next five years [29]. It will be a huge opportunity for companies to produce a magnetic refrigerator for commercial and domestic use. Currently, many companies are working on magnetic refrigerators including Astronautics Corporation of America (ACA), BASF GE, Camfridge Ltd, Cooltech Applications (France), Samsung Electronics Co. Ltd (Korea), Toshiba Corporation (Japan), Vacuumschmelze Gmbh & Co. Kg (Germany).

2.4. Motivation to develop magnetocaloric devices

According to the guidelines of EU, the common refrigerants like R-404a, R-410a, R-134a, R-22, and HCFC-22 (also used as propellant) are banned in vehicles from 1_{st} January 2011 and from 2017 all kinds of these refrigerants are banned in vehicles [30]. Using the Montreal Protocol, countries like China, India and other developing countries have pledged against it. This helped them cut down on the production of the HFCs and CFCs. Keeping the above view in mind the companies needed a new mechanism for refrigeration and magnetic refrigeration is one of those mechanism that can help the countries to achieve that cooling. As the material acts as a regenerator i.e. with magnetic field change cycle cooling effect is produced it makes the magnetic refrigeration a more adequate system than the conventional system. Keeping this in view many companies are working on magnetic refrigeration-based products including electronics to reduce the size of the product that will also make these products more efficient. Also, big markets like China are

requiring more cooling products every year so this technology can be a breakthrough as these countries are not in the favor of using hazardous refrigerants [31].

2.5. Benefits of magnetocaloric devices

The method has clear advantages over conventional refrigeration. The magnetocaloric effect (MCE) is environmentally friendly as it doesn't deplete the ozone layer as compared to the conventional refrigerants, as it does not produce any harmful emissions in the environment. MCE is emerging as an environmentally friendly, in expensive and a low maintenance cost technology. The MCE has less greenhouse emissions than conventional refrigeration. The magnetocaloric device does not produce any harmful HFC's and CFC's making it viable to use in future [32].

Chapter 3

MATERIAL PREPARATION AND

MORPHOLOGY

3. MATERIAL PREPARATION AND PHYSICAL PROPERTIES

3.1. Synthesis

Materials:

Material used for this research is Lanthanum Iron Silicon with Cobalt substitution that is synthesized in Ames Laboratory, US Department of Energy. The material obtained is

La $(Fe_{0.842}Co_{0.073}Si_{0.084})_{13}$ and cobalt composition in the material system is low, a mere 0.07 at%. It is used in the sample to enhance the transition temperature and bring it closer to room temperature. The percentage of Fe, Co, Si and La is 73.05%, 6.68%, 3.66% and 16.61% respectively. The sample is hence forth referred to as La $(Fe_xCo_ySi_{(1-x-y)})_{13}$.

Forms of La $(Fe_xCo_ySi_{(1-x-y)})_{13}$ Samples:

Following samples of La$(Fe_xCo_ySi_{(1-x-y)})_{13}$ were prepared for characterization and measurement of the magnetocaloric effect.

1. Non-milled exposed to air
2. Non-milled exposed to water

3. Milled exposed to air

4. Milled exposed to water

Average size of milled particle is less than 72 microns while average size of particles of non-milled sample is greater than 72 microns. The material was milled using mortar and pestle made up of agate stone. The sample 1 and 3 were kept in air while the sample 2 and 4 were kept in deionized water for 14 days. The main goal for preparation of sample 2 and 4 is to observe its reaction with water as this reaction can change certain properties of the material and water is preferred heat exchange medium for magnetic refrigeration system. These four samples were kept separately in glass bottles as shown in Figure 3.1.
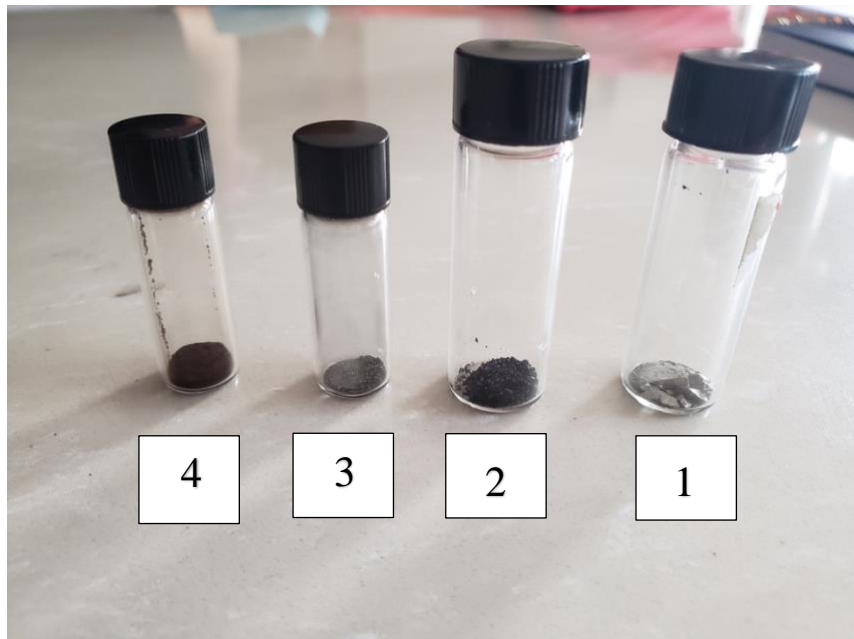
Figure 3.1: Four samples of La(Fe$_x$Co$_y$Si$_{(1-x-y)}$)$_{13}$
(milled air, milled water, non-milled air, non-milled water)

3.2. Sample Preparation

- 4 sample bottles

- SPEX8000 mill

- Fused silica tube

- Annealing equipment

- water-cooled Cu-hearth

- Arc melting apparatus

- Agate mortar

- Argon filled glove box

Arc melting

For the sample preparation the first step is arc melting of elements in this process the vacuum arc melting chamber is first evacuated to create vacuum and then filled with argon gas. The melting of these elements is performed in argon atmosphere. Heat generated by the electric arc struck between the electrode and the metals serves to melt the metals placed in the crucible to form an alloy [33]. A total of 20 g of elements, taken in stoichiometric proportions, were melted together on a water-cooled Cu-hearth. The ingot was re-melted four times and was turned over each time. The total measured weight loss was less than 0.5 wt. %.

Annealing

Annealing is a heat treatment process in which physical, as well as chemical properties of the material, can be changed to improve desired properties like ductility. To change properties, heating

is done above re-crystalline temperature for a certain amount of time to get the desired result. It has three stages.

- Recovery
- Recrystallization
- Grain growth

The as-cast ingot was broken into smaller pieces, which were then wrapped within a tantalum-foil and sealed inside fused-silica tube under vacuum for further heat treatment. The Ingot pieces were annealed at 1050°C for one week followed by quenching in ice-cold water to create thermodynamically stable state.

To avoid the oxidation of the material annealing is done in the presence of forming gas, a mixture of hydrogen and nitrogen, this also avoids the scaling of the material [34]. Annealing is a type of a heat treatment process; different times, temperatures, and quench rates can have very different effects, all of which are unique from one material system to another.

Crushing and Ball Milling

This method is used for the grinding, homogenization, and blending of materials. A mortar and pestle made up of agate stone used to crush the material. The pestle is pressed hard, rotated and grounded to provide the desired powder. Its advantage is that the temperature of the material is not increased and very little energy is used for crushing the material [35]. To obtain the powder, the annealed pieces were crushed in an agate mortar inside an argon-filled glove box and sieved to a uniform particle size of 100μ or below. The powder was then ball-milled in hardened steel

containers using a SPEX8000 mill as shown in Figure 3.2, which is a high-energy ball mill capable of grinding up to 0.2 to 10 grams of dry, brittle samples [36].

Figure 3.2: SPEX8000 Milling Machine [36]

3.3. Scanning Electron Microscopy (SEM)

Scanning electron microscopy also known as SEM is used for the detailed study of a sample's surface. A high-energy electron beam scans the surface of the sample and the interaction of the electron beam with the surface results in secondary electrons. These secondary electrons are collected, processed, and eventually translated as pixels on a monitor to form an image of the specimen's surface topography that appears three dimensional [37]. Figure 3.3 to Figure 3.6 shows the SEM of Lanthanum Iron Silicon Cobalt non-milled and milled samples kept in air. Non-Milled sample's surface is flat as the particle are not broken into piece like milled sample whereas milled sample has broken pieces and greater surface area as compared to the non-milled sample.
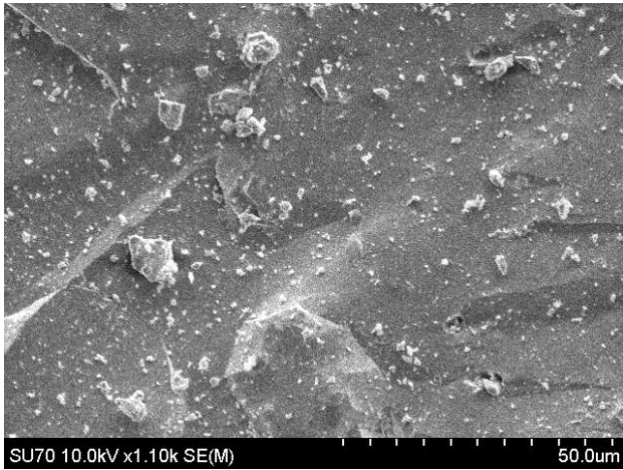
Figure 3.3: SEM of Non-Milled Air Sample of La(Fe$_x$Co$_y$Si$_{(1-x-y)}$)$_{13}$ at 10kV and 50μm
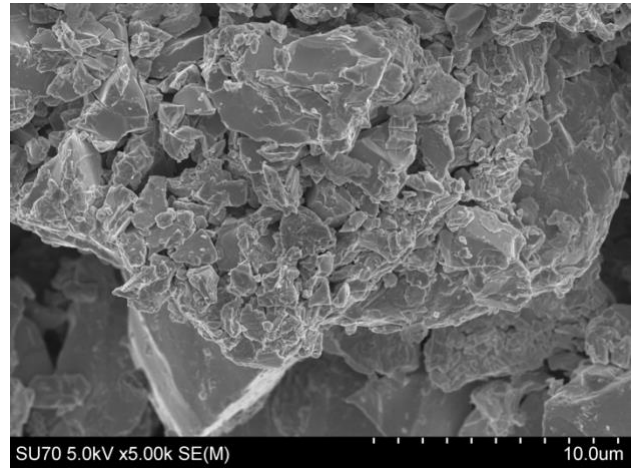
Figure 3.4: SEM of Milled Air Sample of La(Fe$_x$Co$_y$Si$_{(1-x-y)}$)$_{13}$ at 5 kV and 10μm
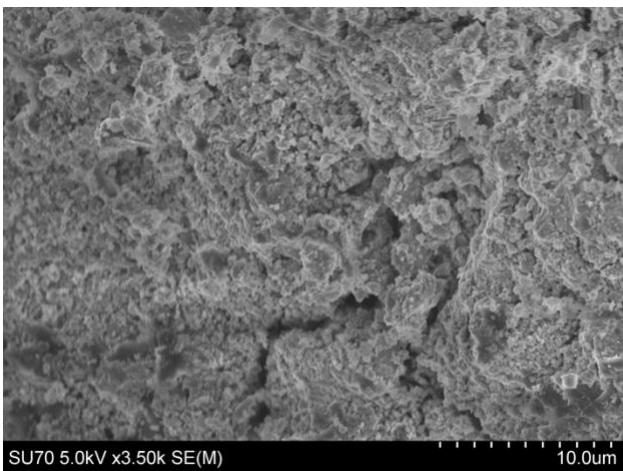
Figure 3.5: SEM of Milled Air Sample of La(Fe$_x$Co$_y$Si$_{(1-x-y)}$)$_{13}$ at 5kV and 10μm
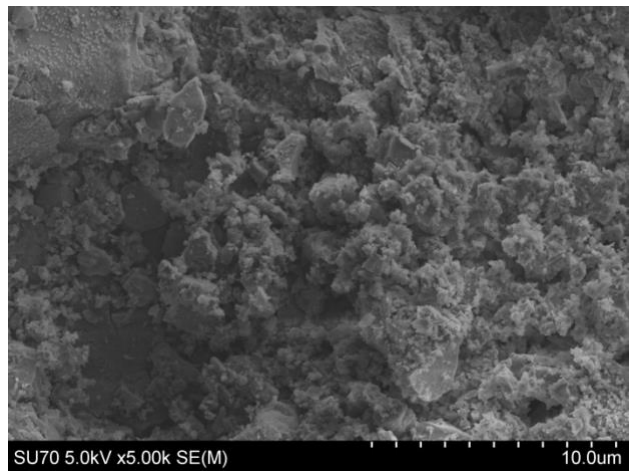
Figure 3.6: SEM of Milled Water Sample of La(Fe$_x$Co$_y$Si$_{(1-x-y)}$)$_{13}$ at 5kV and 10μm

X-Ray Diffraction Analysis (Xrd) of Samples of La(Fe$_x$Co$_y$Si$_{(1-x-y)}$)$_{13}$

XRD analysis is a technique used to study the crystalline structure of a material. Max von Laue, in 1912, discovered that crystalline substances act as three-dimensional diffraction gratings for X-ray wavelengths similar to the spacing of planes in a crystal lattice [38]. PANalytical X'PertPro diffractometer is used to determine crystal structure of the samples. Samples began to lose peaks when contaminated with water as shown in Figure 3.8. Based on this XRay diffraction samples air Non-Milled sample show LaCo$_{13}$ like structure, but the lattice parameters are larger than LaCo$_{13}$ compound. There is a huge peak at 55 deg which may arise from preferred orientation or an impurity that is susceptible to decomposition in air. Water Non-Milled sample show LaCo$_{13}$ like structure but the lattice parameters are larger than LaCo$_{13}$ compound. Except for the 55-degree peak rest of the pattern appears to be more or less similar to as-synthesized material. Water non-milled sample has measurement error that can fixed in future work.
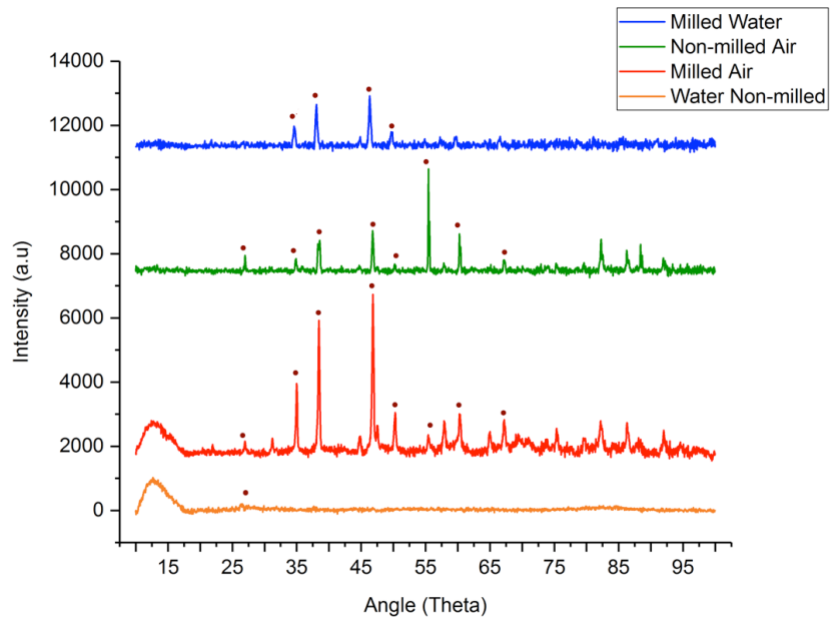
Figure 3.7: X-Ray diffraction patterns of milled and non-milled La(FexCoySi1-x-y)13 samples stored in water and air recorded using Cu Kα radiation

CHAPTER 4

GIANT MAGNETOCALORIC EFFECT

IN La(Fe$_x$Co$_y$Si$_{(1-x-y)}$)$_{13}$

4. GIANT MAGNETOCALORIC EFFECT IN

La(Fe$_x$Co$_y$Si$_{(1-x-y)}$)$_{13}$

4.1. Introduction

The concept of magnetic refrigeration has been around for a very long time and a lot of progress has been made in research of this field. Conventional refrigerators work by compressing and expanding a gas as it flows around the cooling unit, but this process is not especially efficient. Refrigeration currently accounts for 25% of residential and 15% of commercial power consumption in the US In the past it has also used gases harmful to the environment [39]. Scientists and researchers are looking for new magnetocaloric materials with giant magnetocaloric effect, cheaper in cost, higher refrigeration capacity, larger entropy and delta T.

4.2. Magnetocaloric Material Selection

In order to make MCE a commercial technique we need to consider the properties of refrigerants used in it. Gadolinium is currently the benchmark material having curie temperature at room temperature. The pure material cannot be used as a refrigerant, but through alloying its properties are altered to make it viable for refrigeration. Material is selected on various criteria including cooling capacity, life cycle, thermal transport characteristics and efficiency [40]. Figure 4.1 shows the compounds that can be used for the MCE.

From figure 4.1 we can see that La(Fe$_x$Co$_y$Si$_{(1-x-y)}$)$_{13}$ compounds can be used for the commercialization as they demonstrate large MCE at low fields. They have a strong dependence

on Curie temperature of material doped. And most importantly the hysteresis can easily be tuned

by alloying, heat treatment and other types of processing for the customization of the need of the

product. These can be tailored over a relatively large range approaching room temperature.

Figure 4.2 shows the La (FeCoSi) compounds' magnetocaloric abilities in terms of ΔS. It is also

important to consider the price of the compound for practical use. Following figures

demonstrates the viability of La (FeCoSi) compounds as this compound mostly contains iron and

lanthanum therefore it is chosen as material for MCE.
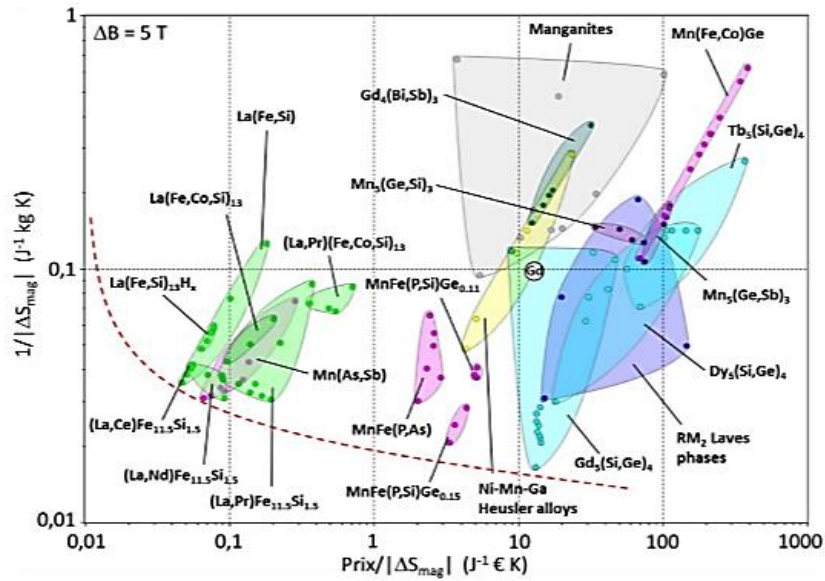
Figure 4.1: Magnetocaloric Characterization [41]
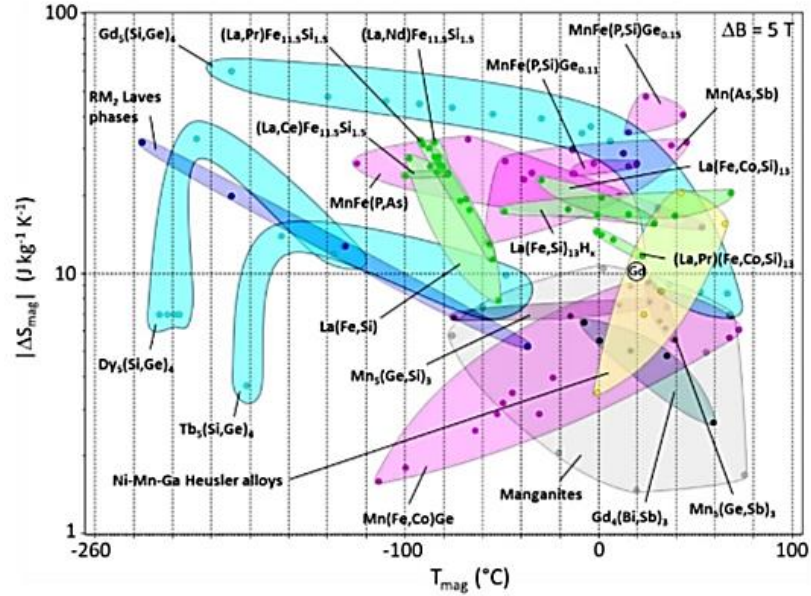
Figure 4.2: Magnetocaloric materials characterization diagram [42]

4.3. Magnetocaloric Refrigerator

Magnetic refrigeration and heat pumping are considered some of the most important alternatives to current vapor-compression technologies, as reported by Brown and Domanski, who have performed a comprehensive comparison of 20 different refrigeration technologies [43]. Despite the fact there has been a lot of research in this field there is still room for more research and progress. LaFeSiCo is one of the most promising magnetocaloric material for refrigeration system as it can produce giant magnetocaloric effect. One of the most promising material displaying giant MCE is the $LaFe_{13xy}Co_yS_{ix}$ (LaFeCoSi) intermetallic compound, where Si is added to stabilize the LaFe13 unstable alloy and Fe substitution with Co increases the Curie temperature (TC) at which the DSM peak is observed without decreasing the MCE [44], [45]. Figure. 4.3 is the schematic diagram of magnetocaloric refrigeration system designed for the Magnetocaloric Cooling Device

2018 at Virginia Commonwealth University. Chapter 6 describes the details of the design shown in Figure 4.3.
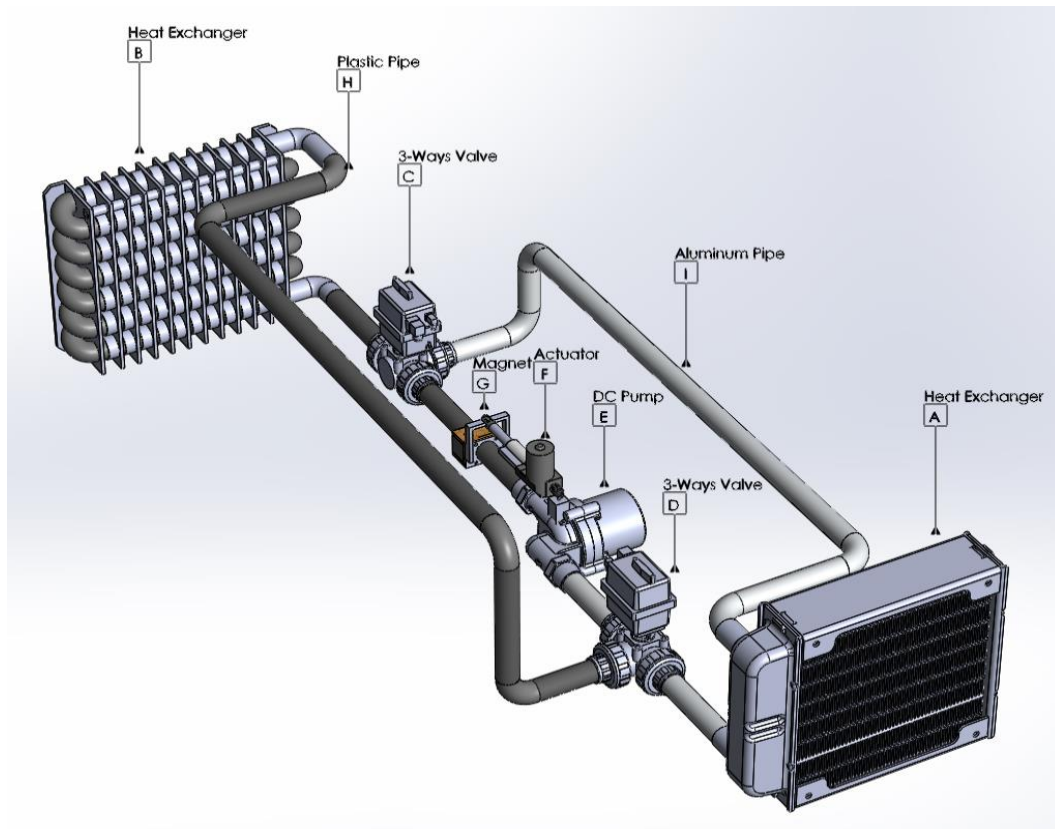
Figure 4.3: Magnetocaloric Cooling Device Design [46]

4.4. Methods of Magnetocaloric Characterization

The magnetocaloric effect of material can be measured by both direct and indirect methods. The direct method is performed by manually applying magnetic field and measuring the change in temperature, although this direct approach is difficult experimentally. There are two major apparatus, DynaCool and VersaLab, which are able to perform indirect MCE measurements such as MT and MH curves. These devices measure electrical, magnetic and thermal properties while

maintaining the temperature and magnetic field applied, allowing us to characterize and benchmark our material relative to other materials.

VersaLab Vibrating Sample Magnetometry by Quantum Design is used for magnetic property characterization of all four samples. Figure 4.4 shows the VSM that is used for magnetocaloric characterization of this sample in Virginia Commonwealth University. With a temperature range of 50 to 400K, this 3-tesla platform is perfect for accomplishing many types of material characterization in a limited space, with no requirements of cryogenic liquids or high-power infrastructure. VersaLab is fully automated turnkey system with a user-friendly interface, and utilizes technology developed for Quantum Design's Physical Property Measurement System (PPMS®) [47].

Figure 4.4: Vibrating Sample Magnetometry

The DynaCool system uses a single two-stage pulse tube cooler to cool both the superconducting magnet and the temperature control system, providing a low vibration environment for sample measurements [48]. For this research DynaCool is used for characterization of high temperature behavior and heat capacity of the samples. Dynacool can achieve high vacuum ($\sim 10^{-5}$ Torr) needed for measuring heat capacity. Without proper vacuum heat can transfer through the environment, invalidating the assumption of adiabatic conditions needed for this measurement. Figure 4.5 is DynaCool located at VCU NCC Nano materials Core Characterization Facility used for the characterization of LaFeSiCo.
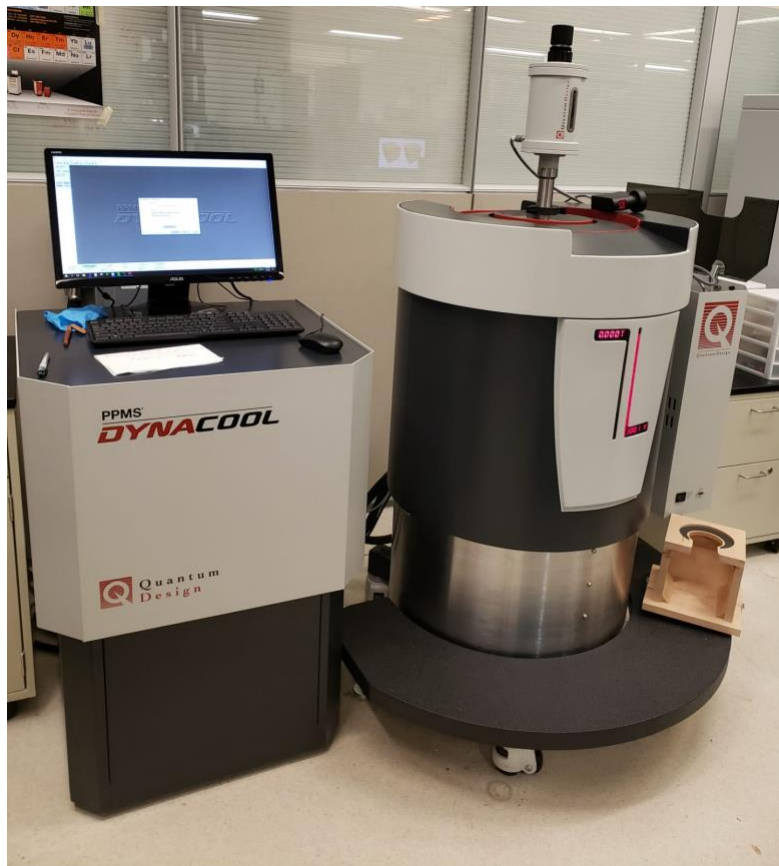
Figure 4.5: PPMS Dynacool in Nano Characterization Center (NCC)
Virginia Commonwealth University

4.5.   Estimation of Magnetocaloric Effect Using M-H and M-T Curves

All ferromagnetic material exhibits some type of magnetocaloric effect depending on their physical and chemical properties which can be characterized using magnetization vs applied field (M-H) and magnetization vs temperature (M-T) measurments.   In order to measure this experimentally, the sample is fixed on a non-magnetic rod that vibrates between the measurement coils, generating an electrical current which is related to the sample's magnetization. For this research VersaLab Quantum Design-cryogen-free is used for magnetic characterization of $La(Fe_xCo_ySi_{(1-x-y)})_{13}$ with temperature range of 50 – 400K and the maximum magnetic field of 3 Tesla. The sample is weighed and enclosed in a plastic capsule which is inserted in a half brass tube. This brass tube is placed in the sample mounting station to make sure the sample within the plastic capsule is at 35 mm from the bottom of the tube, which ensures the sample will fall within the center of the measurement coils. With the help of the rod, the brass half tube is mounted inside
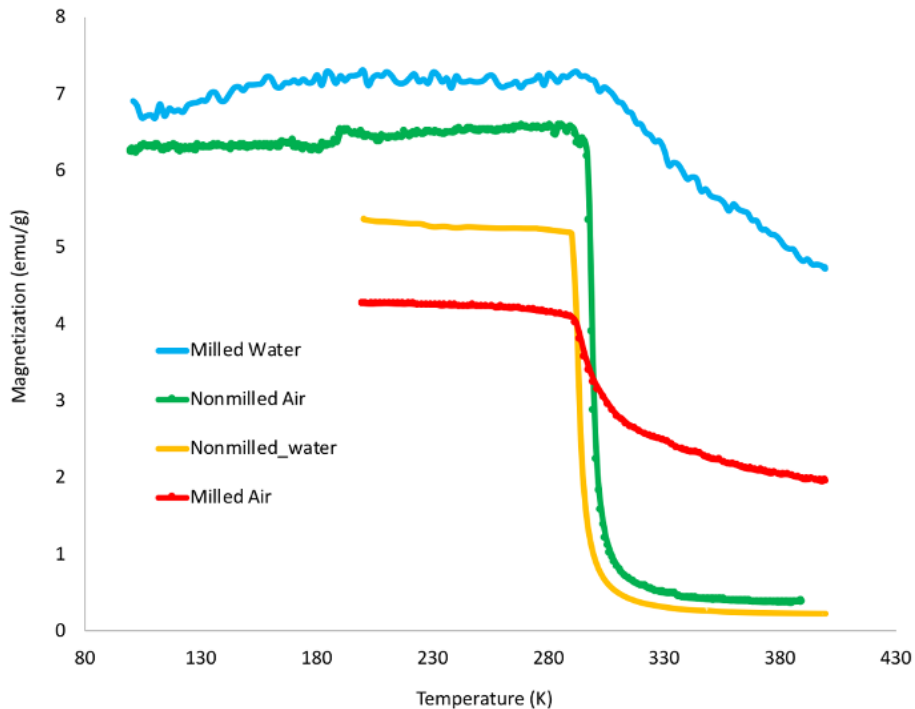
the chamber. Following Figure 4.6 represents the relationship of magnetization vs temperature for all the samples at 0.01 Tesla magnetic field.

Figure 4.6: Magnetization vs Temperature at 0.01 T

Milled water has highest magnetization, but it has a broadened transition, whereas the non-milled air sample has sharpest transition among all. Close to 300K for all samples there is a transition from ferromagnetic $La(Fe_xCo_ySi_{1-x-y})_{13}$ phase to paramagnetic $La(Fe_xCo_ySi_{1-x-y})_{13}$ phase making it the transition temperature of the material. Both milled samples show an incomplete transition and retain large magnetization even beyond 400K, which could be due to the contamination of iron from the steel ball milling. The results of these magnetic measurements were later used for the calculation of entropy by substituting these results into Maxwell's equations.

Magnetocaloric material's behavior at transition temperature is one of the key discussions when it comes to characterization of the MCM, as at this temperature material goes through change in their magnetic properties and the magnetocaloric effect is greatest. Figure 4.7 represents the
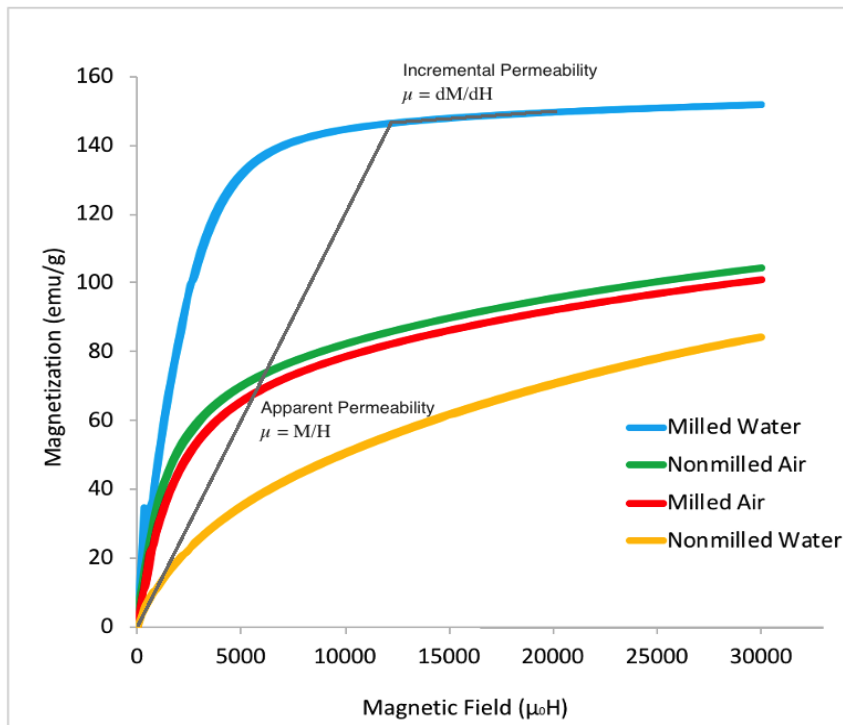
Figure 4.7: Magnetization vs Magnetic Field at 300K of
$La(Fe_xCo_ySi_{(1-x-y)})_{13}$

magnetization vs magnetic field relationship of LaFeSiCo at the transition temperature of 300K.

From Figure 4.7 it can be seen that the MH curves shows soft magnetic material behavior which

makes them easy to demagnetize. The MH curves for LaFeSiCo show approximately no applied

field is required to demagnetize the material, which makes them feasible to use for the repeated

magnetization and demagnetization cycles required for a magnetocaloric refrigeration device.

The milled water sample shows higher magnetization and higher permeability as compared to the

La(Fe$_x$Co$_y$Si$_{1-x-y}$)$_{13}$ sample kept in air which is due to the formation of magnetic phase in the

water sample. Figure 4.8 shows magnetization vs magnetic field at 275 K for all the samples the

curves are close to each other whereas at 300K temperature milled water has the highest

magnetization.
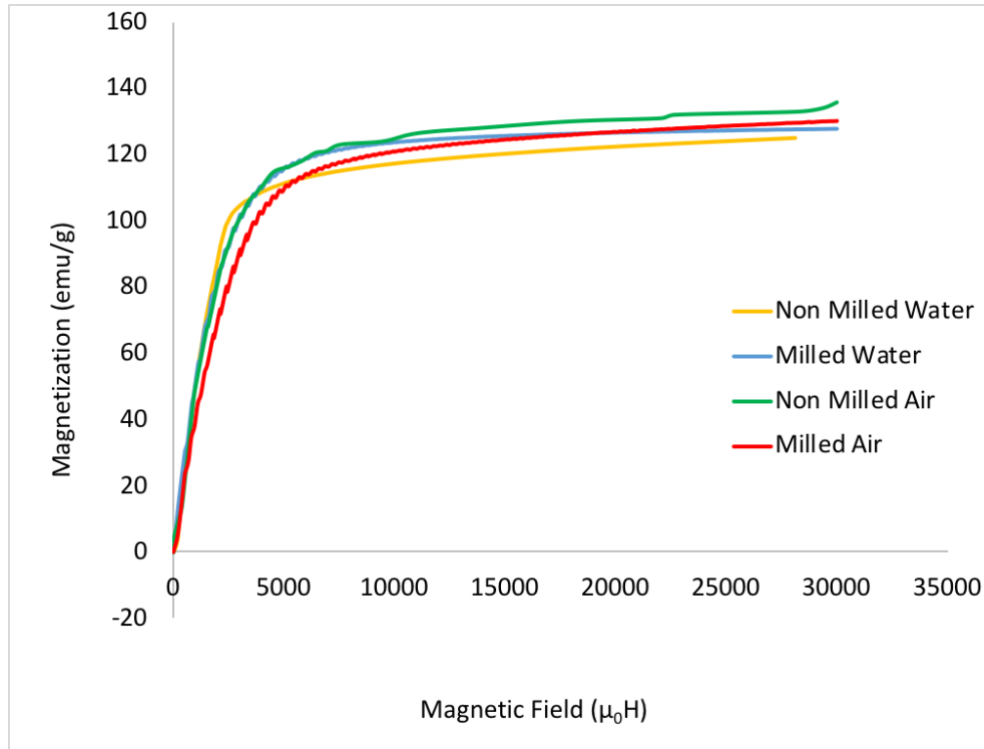
Figure 4.8: Magnetization vs Magnetic Field of
La(Fe$_x$Co$_y$Si$_{(1-x-y)}$)$_{13}$ at 275 K

4.6. Transition Temperature of La(Fe$_x$Co$_y$Si$_{(1-x-y)}$)$_{13}$

In the literature, the intrinsic i.e. inherent magnetic property (Tc) has been studied by Buschow et al. [49], in order to better understand the extrinsic magnetic properties of the material magnetization vs temperature relationship is also plotted at high temperature range that is from 300 K to 1000 K at 0.01 Tesla applied magnetic field. From Figure 4.9 the transition temperature of Lanthanum Iron Silicide Cobalt can be observed. Iron (III) oxide Fe$_2$O$_3$ is antiferromagnetic below ~260 K (Morin transition temperature) and exhibits weak ferromagnetism between 260 K and the magnetic ordering temperature 950 K [50]. The nonmilled water sample transition near 950 K may be indicative of formation of iron (III) oxide in the sample.
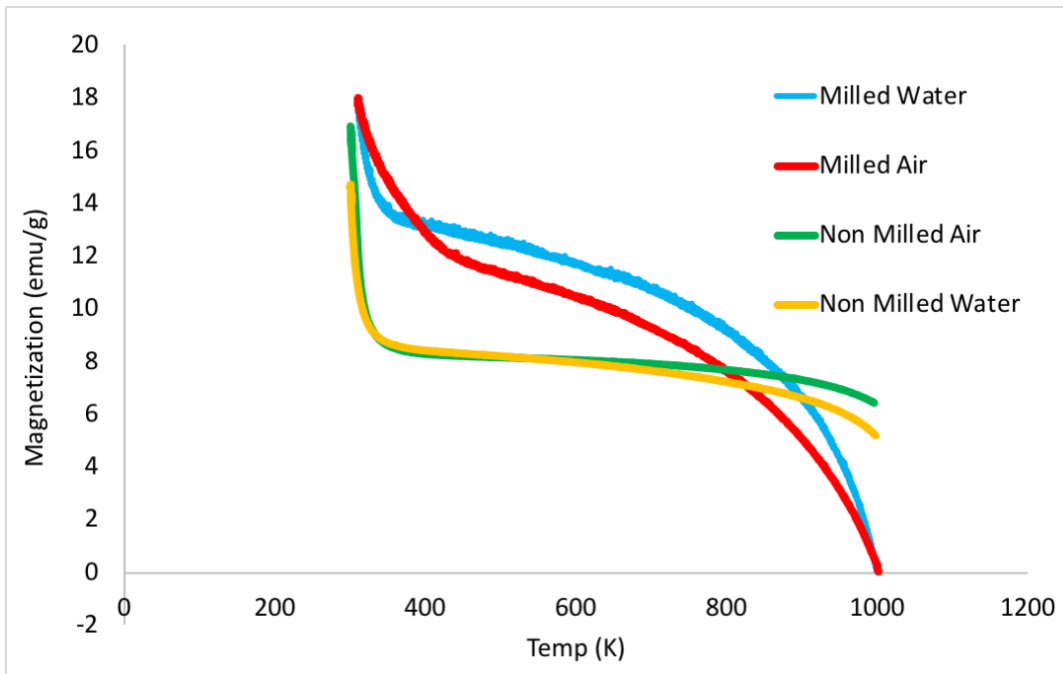
Figure 4.9: Transition Temperature of La(Fe$_x$Co$_y$Si$_{(1-x-y)}$)$_{13}$

at high temperature 300K – 1000K

Milled sample results are normalized to calculate their mass and they don't have sharp transition as non-milled samples. On comparison of Figure 4.6 and Figure 4.9 it can be concluded that milling has broadened the transition which can be due to contamination of iron from steel ball milling and due to milled particle size broadening of transition can be observed.

4.7.   Arrott Plot of LaFeSiCo from magnetization isotherms

Figure 4.10 shows the Arrott plot with isothermal magnetization curves of La(Fe$_x$Co$_y$Si$_{(1-x-y)}$)$_{13}$ non-milled water sample measured with the temperature range of 250 K to 320 K with interval of 5 K. Arrott plots can be used for analysis of magnetic properties of magnetocaloric materials, These plots are an alternative means of viewing critical behavior of sample at transition

temperature. The slope of each isotherm at given temperature can be found using following equation

$$\text{Slope} = M_2 \left(\frac{H}{M} \right) \qquad\qquad (4.1)$$

Arrott plots can benefit to understand if magnetocaloric material is going through first order or second order phase transition. Both transitions have their own advantages and disadvantages, FOPT materials have large magnetic entropy and temperature change but goes through thermal hysteresis while on the other hand SOPT usually have smaller magnetic entropy as compared to the FOPT but doesn't go through thermal hysteresis. Therefore, a current goal is to combine the best from both types of materials: large response without hysteresis and a tradeoff between static and cyclic performance [51].

The search for such materials bring forth the intermediate point of FOPT converting to SOPT, which is usually termed tricritical point in literature though the critical point of the SOPT will be
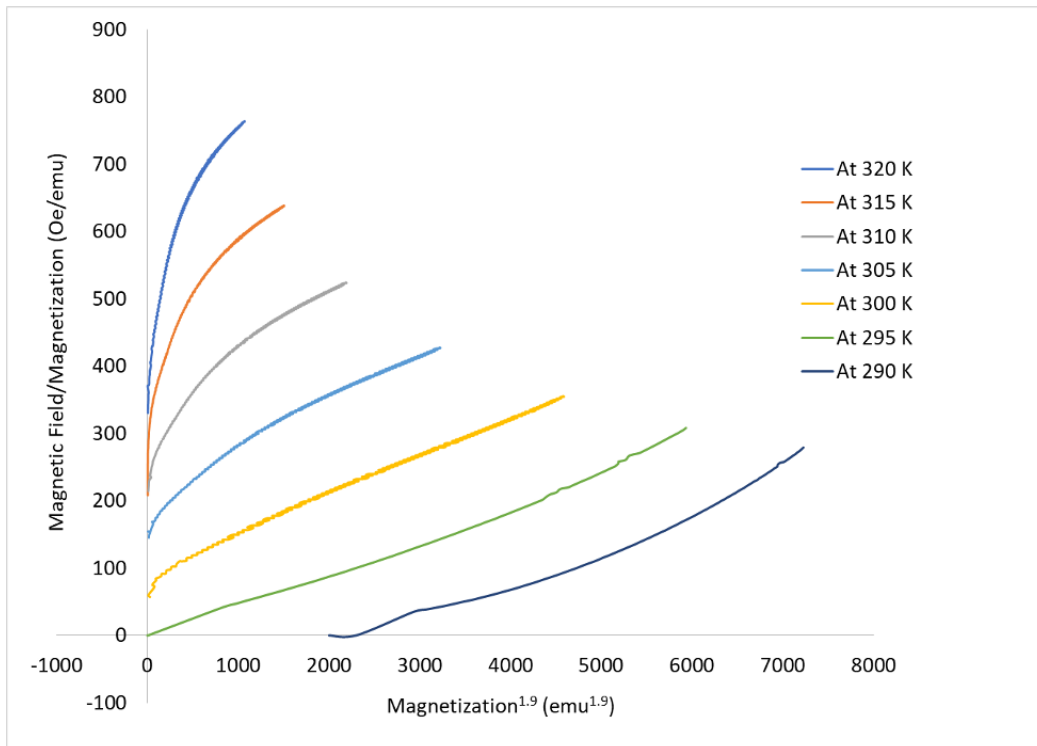
Figure 4.10: Arrott plot of Non-Milled Water
La(Fe$_x$Co$_y$Si$_{(1-x-y)}$)$_{13}$ Sample

more appropriate. LaFeSi and MnFePSi-type13 alloy series are examples exhibiting a gradual change from FOPT to SOPT [52]–[54]. From above mentioned figure it can be seen that curve at 295K passes through the origin of the arrott plot showing that 295K is the transition temperature of the material. FOPT material's arrott plot exhibits negative slope while SOPT material's arrott plot exhibits positive slope. Following Table 4.1 represents the slope of each LaFeCoSi arrott plot curve

Table 1: Slope of Non-Milled water sample Arrott Plot

Temp(K)	Slope
320	2.55
315	4.24
310	7.55
305	12.16
300	17.02
295	18.90
290	18.47

Positive slope of the arrott plot represents that material is SOPT which means it will not go through thermal hysteresis, which makes it a suitable choice magnetocaloric refrigeration prototype design.

CHAPTER 5

CHANGE IN ENTROPY AND

TEMPERATURE

5. CHANGE IN ENTROPY AND TEMPERATURE

5.1. Introduction

Entropy of magnetocaloric materials is the integral part of magnetocaloric effect. When in a controlled system external magnetic field larger than saturation magnetic field is applied, the temperature of ferromagnetic materials changes. This change of temperature takes place due to the change in the entropy of the material which can be calculated. The factors that contribute to the total summation of entropy of a magnetic material are lattice entropy, magnetic moment entropy and entropy of electron conduction. Therefore, total entropy of magnetic material at given temperature and magnetic field can be written as shown in Equation 5.1. At constant pressure this total entropy of the material depends upon the temperature and the magnetic field.

$$\Delta S(T,H) = \Delta S_m(T,H) + \Delta S_l(T) + \Delta S_e(T) \tag{5.1}$$

Where,

S_m is the magnetic entropy

S_l is the lattice entropy

S_e is the electron entropy

The temperature of an adiabatic system will increase in response to an applied magnetic field. This increase in temperature is due to the fact that with application of magnetic field ΔS_m is decreased and in order to maintain a constant total entropy the temperature must rise. On the other hand, when magnetic field is applied to the isothermal system meaning the temperature remains constant,

the entropy of the system decrease. This decrease in entropy is due to the decrease in the magnetic entropy of the material. As shown in figure 5.1
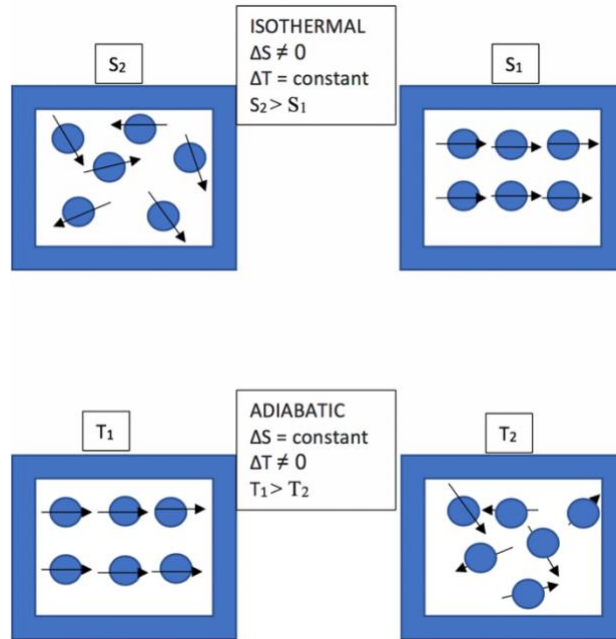
Figure 5.1: Isothermal and Adiabatic Processes

These isothermal and adiabatic processes are the key component of the magnetocaloric theory. This can be explained using thermodynamics and Maxwell's equations. Percharsky el al plotted the entropy vs temperature representing magnetocaloric effect of a material in zero(S_0,T_0) and non-zero (S_1,T_1) magnetic field [9]. In Figure 5.2 solid line represents the total entropy, dotted line represents the summation of lattice and electronic entropy while the dashed line represents the magnetic entropy.
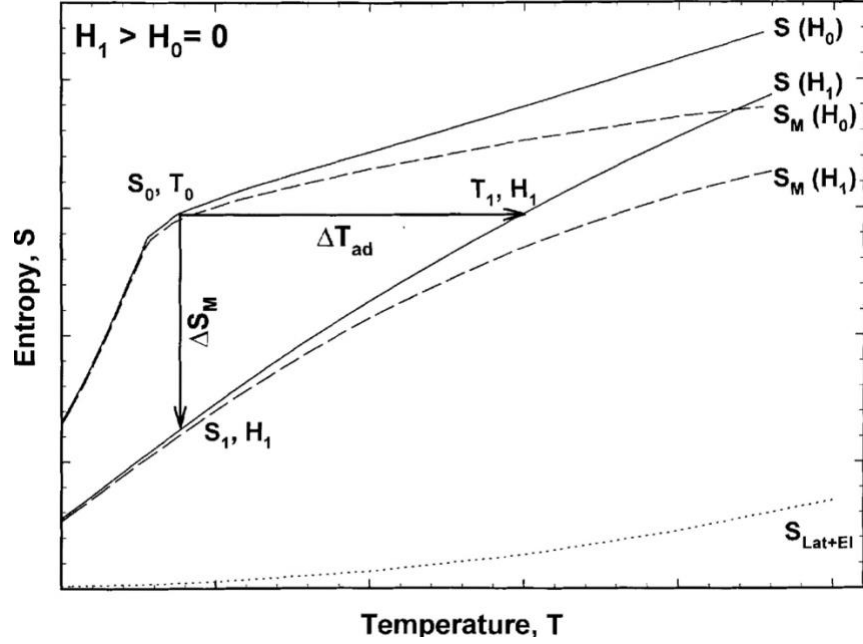
Figure 5.2: Schematic Diagram of Entropy (S) vs Temperature (T) [9]

The basic relationship between applied magnetic field, magnetization and temperature of the material is explained by Maxwell equations [55]

$$\left(\frac{\partial S(T,H)}{\partial H}\right)_T = \left(\frac{\partial M(T,H)}{\partial T}\right)_H \tag{5.2}$$

Integrating Eq. 5.2 with respect to the magnetic field gives

$$\Delta S_m(T, \Delta H) = \int_{H_1}^{H_2} \left(\frac{\partial M(T,H)}{\partial T}\right)_H dH \tag{5.3}$$

5.2.   Measurement of Change in Entropy Using Maxwell Relations

Change in entropy can be calculated using the integrated Maxwell's Equation 5.3. can be solved for experimental data using numerical integration approaches [56]. Resultant entropy changes for La (Fe$_x$ Si$_{1-x}$)$_{13}$ compounds with x=0.88, 0.89 and 0.90 plotted against temperature with an external magnetic field ranging from 0 to 5T results in Figure 5.3 [57].
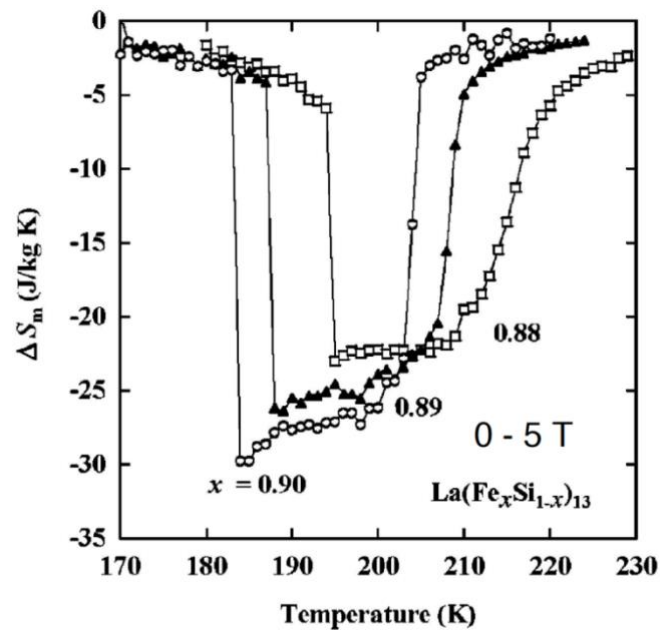
Figure 5.3: Entropy changes (ΔS) for Lanthanum
Iron Silicon vs Temperature (K) [57]

Using Equation 5.3 the change in entropy over a 3T change in magnetic field was calculated for the four experimental groups discussed previously, the results of which are plotted in Figure 5.4.
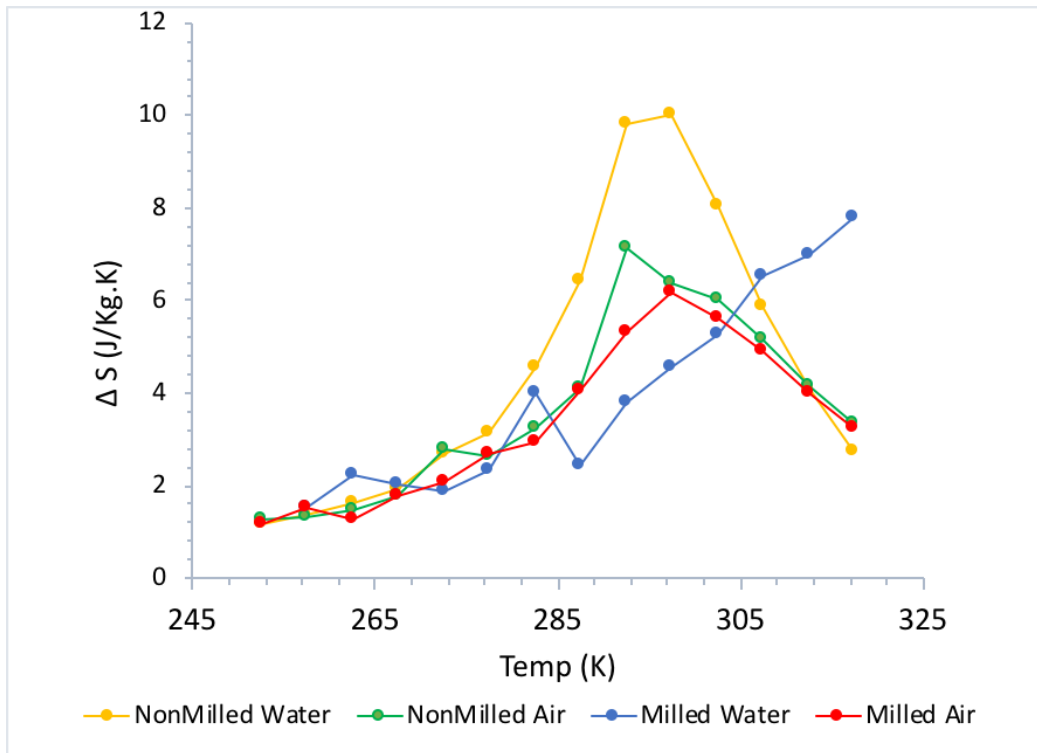
Figure 5.4: Change in Entropy(ΔS) vs Temperature (T) for LaFeSiCo using Maxwell Relation

As the non-milled sample stored in water has a sharper transition near 300 K for magnetization vs magnetic field (Figure 4.5) therefore the change in entropy represents the maximum ΔS of 10.3 J/Kg.K at 297.5 K among all samples. For milled sample stored in water the maximum delta S is 4 J/Kg.K because milling has significantly broadened its transition that resulted in low entropy change. The highest observed change in entropy of non-milled water sample makes it a better selection for the new magnetic refrigeration systems out of the samples tested. The new magnetic refrigeration device only relies on running water and utilizes basic components such as pumps,

valves, all of which are relatively inexpensive and can easily be replaced or fixed. The initial design for this refrigeration system was proposed by team at VCU and this characterization of $LaFe_{x}CO_{y}Si_{13-x-y}$ is used to design new refrigeration which will be more efficient. Figure 5.5 show SolidWorks 2D drawings of initial design. Hot water and cold-water cycle are above and below the magnetocaloric material respectively. 3-way solenoid valve are programmed and tuned with time. These valves are also synced with Arduino to control the opening and closing of valves. Every time cycle is reversed there is a chance of mixing hot side water in your cold-water side that can affect the efficiency. This is one of the potential errors in the design that can be worked on in future to maximize the efficiency.
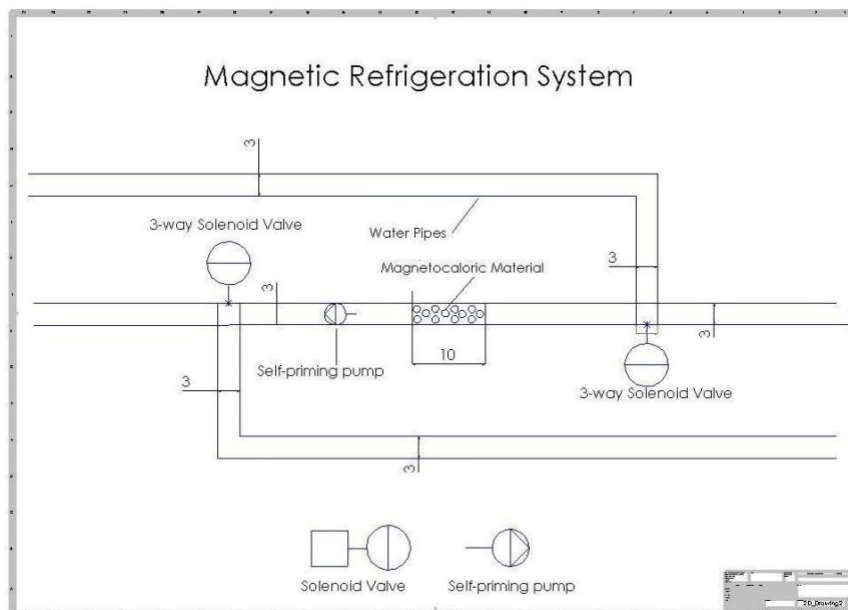
Figure 5.5: Magnetic Refrigeration System Design in Solid Works [46]

5.3. Measurement of Heat Capacity

Heat capacity is the physical property of the material, describing the amount of heat required to increase the temperature of the sample by one unit. The SI unit of heat capacity is J/K and it is measured using Dynacool at constant pressure. The heat capacity of a material depends on variety of factors like temperature, volume, pressure and phase transition. Heat capacity of a magnetocaloric material can be used to indirectly quantify about its magnetocaloric effect. The isothermal entropy and the adiabatic temperature change are related via the heat capacity C_P, as shown below [58]

$$\Delta \text{Tad} \approx \frac{-T \ \Delta \text{S}}{Cp} \tag{5.5}$$

As it can be seen from Equation 5.5, change in temperature is inversely proportional to the heat capacity of the material. This change of temperature is the crucial part of any magnetocaloric refrigeration system, decrease in heat capacity results in increase of change in temperature. Figure 5.6 represents the heat capacity of non-milled water Lanthanum Iron Silicon Cobalt with lower heat capacity materials enabling more efficient refrigeration. This analysis is crucial to prototype magnetocaloric refrigeration design as it will feed to the calculation of change in entropy and change in temperature. Figure 5.7 represents the heat capacity of non-milled air sample of LaFeSiCo kept in air. Heat capacity measurements are not completed on milled samples for the reason sample needed to be prepared carefully so that, it is not lost in the device and heat is transferred equally between the particles.
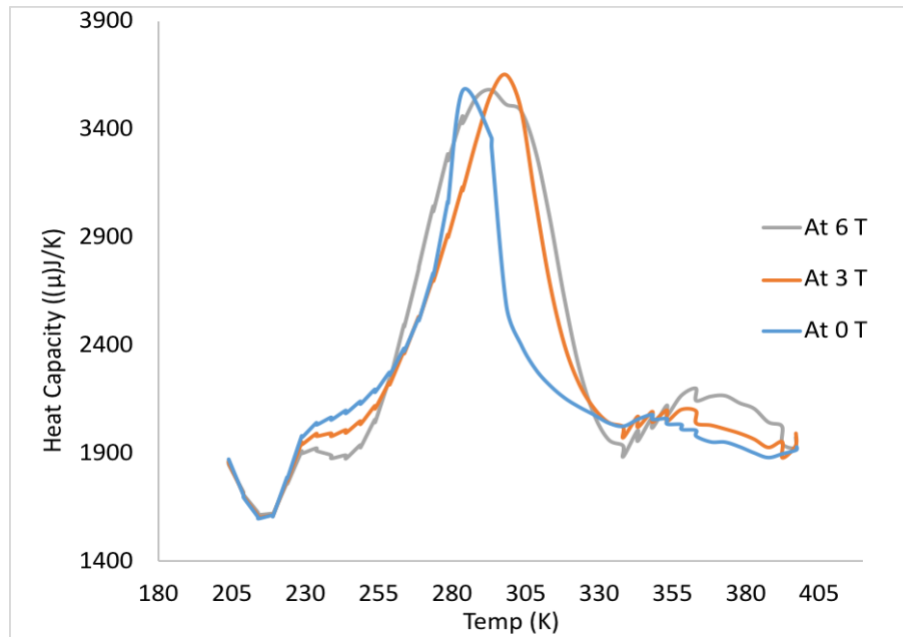
*Figure 5.6: Heat capacity of Non-Milled Air LaFeSiCo as a
function of temperature under different applied magnetic fields*
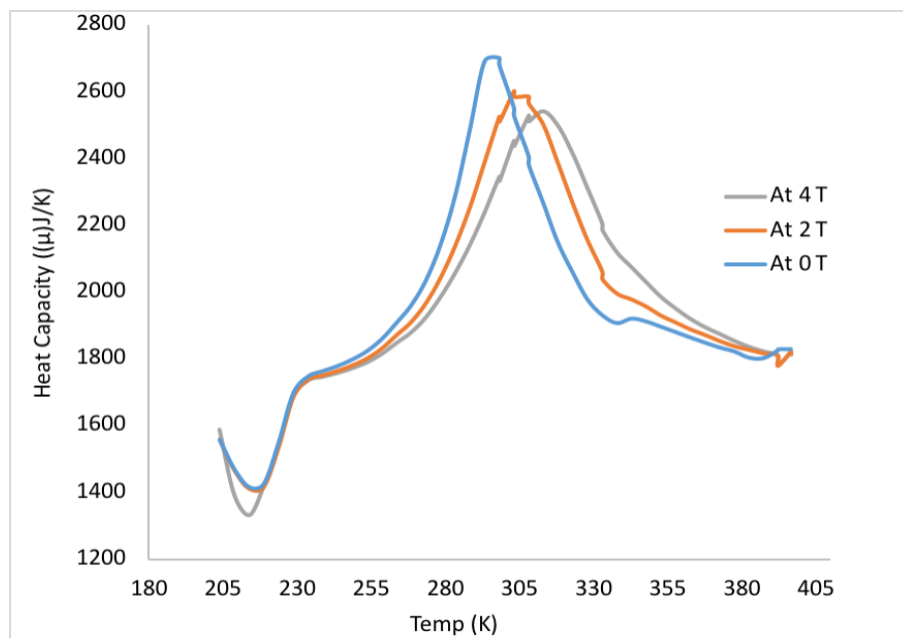
*Figure 5.7: Heat capacity of Non-Milled Water LaFeSiCo as a function of
temperature under different applied magnetic fields*

When Figure 5.6 and Figure 5.7 are compared, the heat capacity of non-milled water is lower in comparison to non-milled air sample. Figure 5.8 represents the comparison of heat capacity vs temperature at 3 Tesla magnetic field for non-milled sample kept in air and water. These measurements are completed on 3 Tesla change of magnetic field as magnetocaloric refrigeration is prototyped with 3 Tesla permanent magnet. It is very clear from the graph that non-milled water sample with lower heat capacity has great potential for magnetic cooling devices. Next section will explain more about calculation temperature change when applied magnetic field is changed.
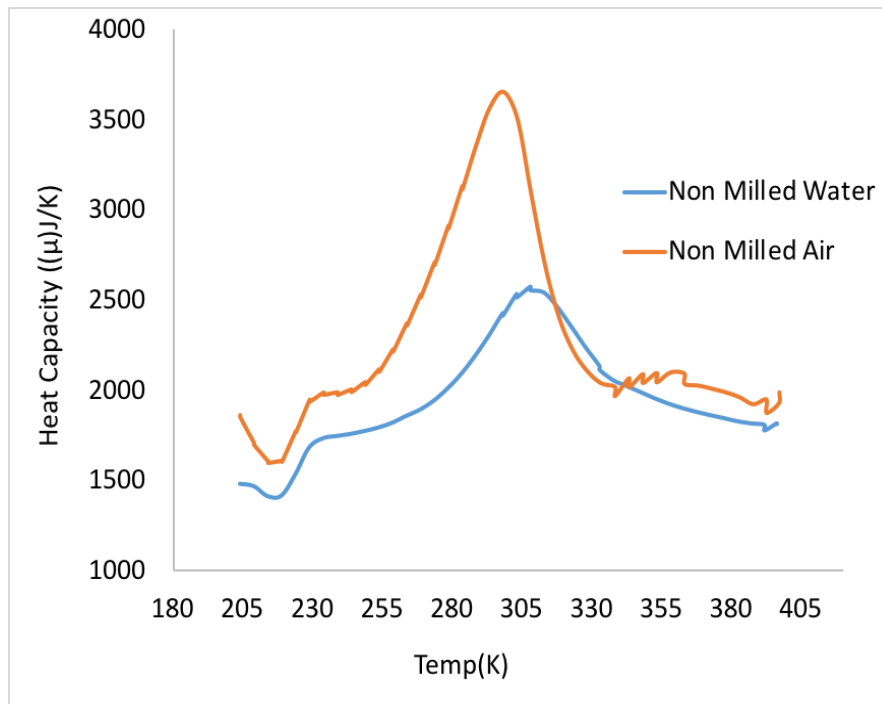
Figure 5.8: Comparison Analysis of Heat Capacity vs Temperature
of Non-Milled Air and Water LaFeSiCo at Magnetic Field change of 3T

5.4. Entropy Change using Heat Capacity

Total entropy of a material is dependent on the temperature with constant magnetic field. Figure 5.9 represents the total entropy vs temperature for a simple ferromagnet. Negative delta S in red colored arrow shows the magnetocaloric effect of the material. Blue arrow towards right represents the change in temperature due to magnetocaloric effect. Isothermal entropy can be determined using heat capacity data with the help of following equation at applied magnetic field where S_0 is the entropy at 0 K and S_{OH} is entropy at 0 K and H field [59]

$$S(T)_{H=0} = \int_0^T \frac{C(T)}{T} dH + S_0 \tag{5.6}$$

$$S(T)_{H\neq0} = \int_0^T \frac{C(T)}{T} dH + S_{0,H} \tag{5.7}$$
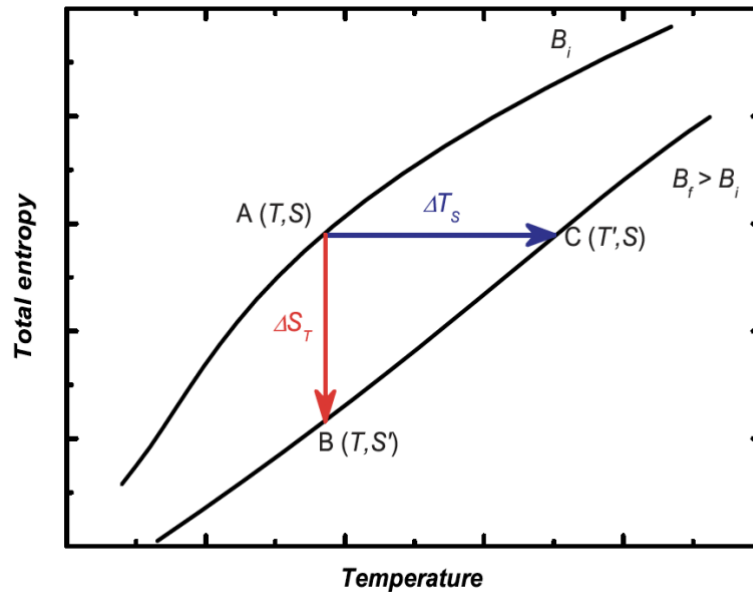
Figure 5.9: Total Entropy vs Temperature for
a simple ferromagnet at constant field Bi and Bf [60]

The entropy change ΔS of a system in a temperature range from T_1 to T_2 are given by

$$\Delta S(T_1 \text{ to } T_2) = \int_{T(1)}^{T(2)} C_p \, dT \tag{5.8}$$

Equation 5.8 can be used to calculate the change in entropy using heat capacity data. Heat capacity vs temperature and magnetization vs magnetic fields graphs were plotted at different magnetic fields to further calculate the ΔS for these samples. Change in entropy can be calculated using following formula

$$S(T,H) - S(T_0) = \int_{T_0}^{T} \frac{C_p(T',H)}{T'} \, dT' \tag{5.9}$$

Following standard calculation method is used to calculate change in entropy at specific magnetic field.

<p align="center">Table 2: Change in Entropy at Specific Magnetic Field</p>

A	B	C	D
Sample Temp. (K)	Heat Capacity (J/K.Kg)	Column B/Coulmn A	Integrate column C for x = (Highest Temp, Lowest Temp)
396	592.25	1.49	

Following function can be used in origin to integrate column C
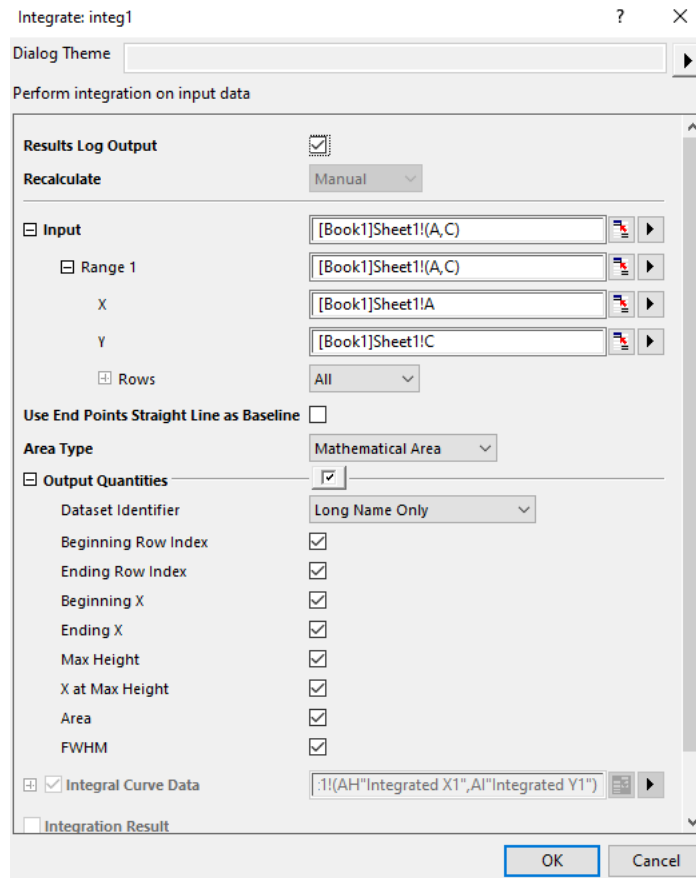
Figure 5.10: Origin Integration function for change in entropy calculation

Figure 5.10 and 5.11 represents the relationship between ΔS(J/Kg.K) and temperature (K) for non-milled sample stored in air and water using heat capacity data at magnetic fields of 0,3 and 6 T. Non-milled sample stored in water has the maximum Δ S at 6T. On comparison of Figure 5.8 to the Figure 5.10 and 5.11 it can be seen that values of ΔS at 3T calculated using magnetization and heat capacity measurements are close to each other for non-milled samples. Addition of deionized water to the non-milled samples has increased the magnetization that can be due to the formation of ferromagnetic phases of Fe_3O_4. Considering increased entropy of non-milled water sample calculated from magnetization and heat capacity measurements, water can be used as a heat transfer fluid for magnetic cooling refrigeration systems. One of the problems that can arise is deterioration of material when kept in water for long time. In future work material can be coated with some type of coating to inhibit the deterioration.
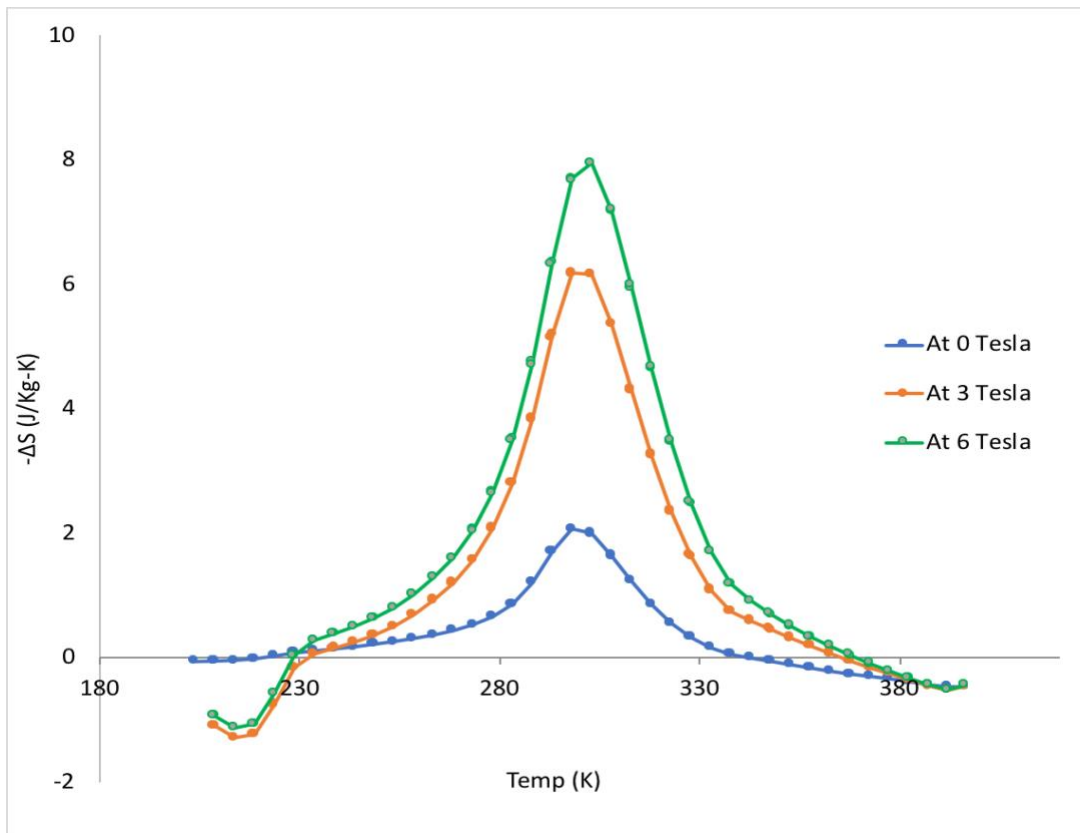
Figure 5.11: ΔS vs T of Sample Stored in Air Using Heat Capacity
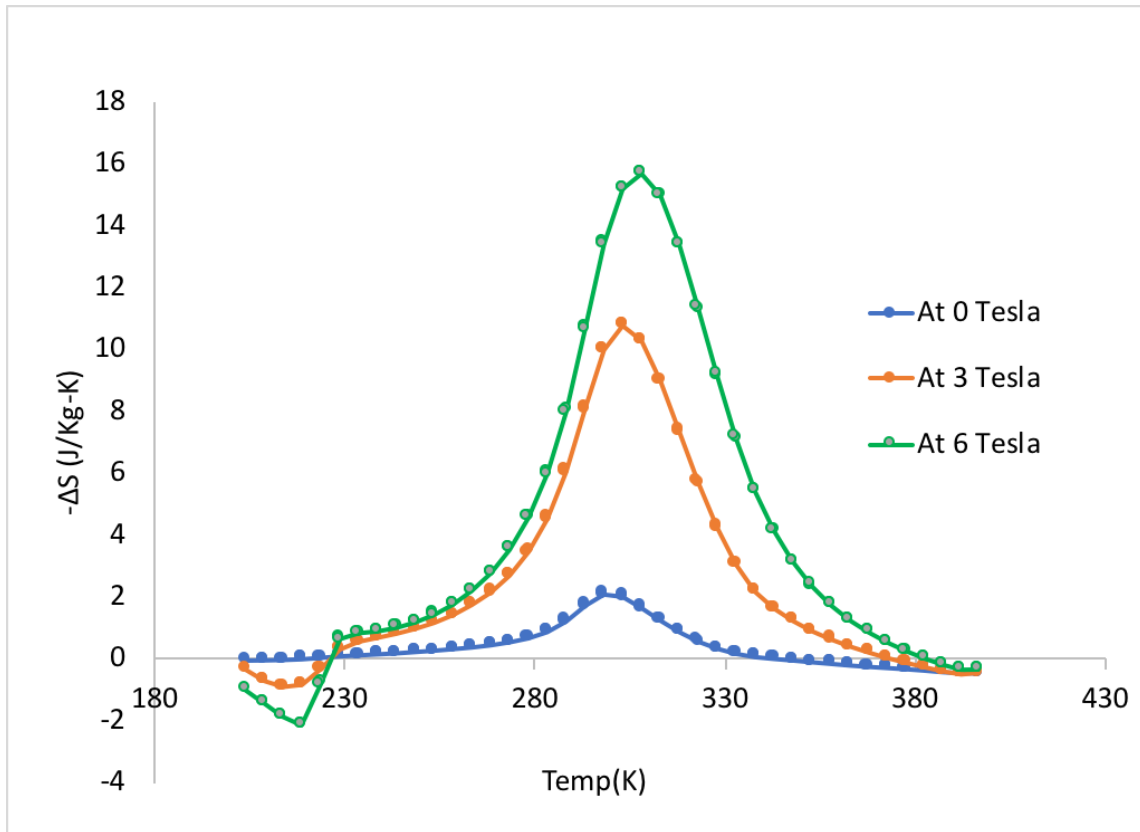
Figure 5.12: ΔS vs T of Sample Stored in Water Using Heat Capacity

5.5. Measurement of Change in Temperature Using Heat Capacity Data

When an external magnetic field is applied to the sample, the change in temperature of sample from initial temperature (T_0) to final temperature (T_F) can be calculated by direct and indirect methods. Direct change in temperature can be calculated by temperature sensor that measure the temperature when magnetic field is rapidly changed from initial magnetic field (H_0) to the final magnetic field (H_f). The measurements can be carried out either on immobilized samples by changing the field [61] or by moving the sample in and out of a constant magnetic field region [62].

In adiabatic condition i.e. total entropy is kept constant when magnetic field is applied magnetic entropy decreases and this relationship can be written as

$$S\,(T_0,\,H_0) = S\,(T_1,\,H_1) \tag{5.5}$$

As total entropy doesn't change, this change in magnetic entropy results in temperature increase. This adiabatic rise in temperature can be written as

$$\Delta T_{ad} = T_1 - T_0. \tag{5.6}$$

Using the thermodynamic relationship given below [55]

$$\left(\frac{\partial T}{\partial H}\right)_S = -\left(\frac{\partial S}{\partial H}\right)_T \left(\frac{\partial T}{\partial S}\right)_H \tag{5.7}$$

$$C_H = T\left(\frac{\partial S}{\partial T}\right)_H \tag{5.8}$$

Where C_H is the heat capacity at constant magnetic field. With the help of equation 5.2 adiabatic temperature can be calculated as

$$dT_{ad} = -\left(\frac{T}{C(T,H)}\right)_H \left(\frac{\partial M(T,H)}{\partial T}\right)_H dH \tag{5.9}$$

Change in temperature at applied magnetic field is given by

$$\Delta T_{ad}(T,\,\Delta H) = \int_{H_1}^{H_2} \left(\frac{T}{C(T,H)}\right)_H \left(\frac{\partial M(T,H)}{\partial T}\right)_H dH \tag{5.10}$$

This equation can be simplified and written as

$$\Delta T_{ad} = \int_{H_1}^{H_2} \frac{T}{Cp} \left(\frac{\partial M}{\partial T}\right)_H dH \qquad (5.11)$$

Using Equation 5.11 adiabatic temperature change of LaFeSiCo is calculated as follows where mass of sample is 0.0175 g.

Table 3: Adiabatic Temperature Change Calculation with Heat Capaicty and Entropy Data

A	B	C	E	F	G
Temp(K)	ΔS (J/Kg.K) From 0 to 3 Tesla	C_p (J/K) at 3 Tesla	Temp(K)/C_p(J/K) At 3 Tesla	Delta T (K/Kg) From 0 to 3 Tesla	Delta T (K) From 0 to 3 Tesla
			Col A/Col C	Col E * Col B	Col F * mass in g
292.5 (K)	7.1446 (K/Kg.K)	0.013204 (J/K)	22152.19 (K_2/J)	158.8707 (K/Kg)	2.7627 (K)

Figure 5.12 represents the change in temperature of 3.6 K for non-milled water sample with change in applied magnetic field from 0 to 3 T while the change in temperature for non-milled air sample is 2.8 K. This analysis concludes that maximum change in temperature for refrigeration device based on LaFeCoSi with change of 3T will be close to 3.5 K and for future research it can be

investigated how can we maximize this change in temperature with the variation of applied magnetic field.
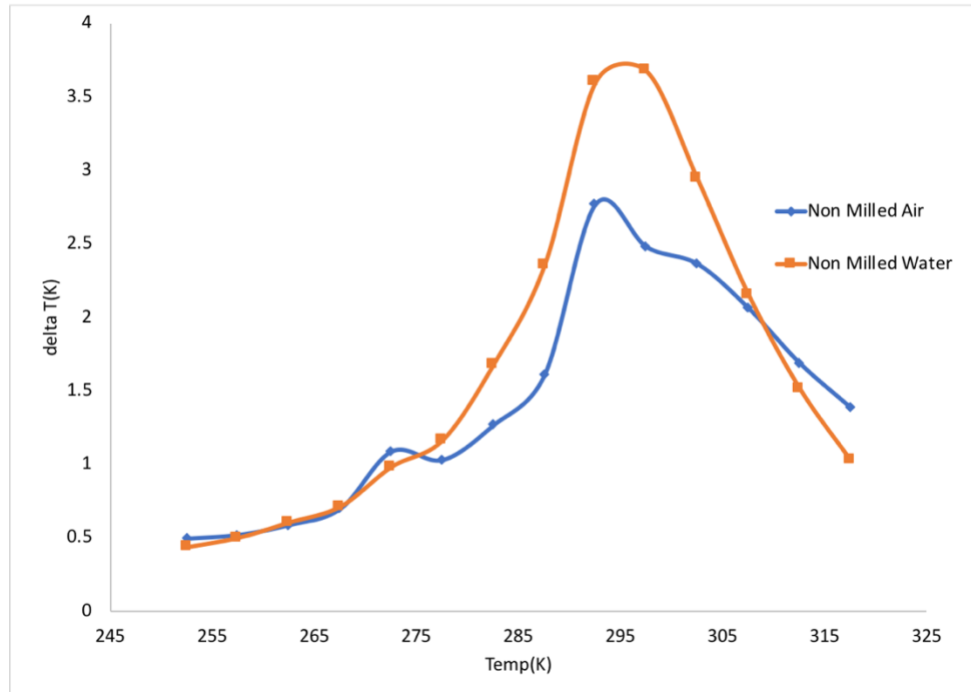
Figure 5.13: The adiabatic temperature change for non-milled water and air sampled in the temperature range from ~250 K to ~320 K, for a magnetic field change between 0 and 3 T

CHAPTER 6

MAGNETOCALORIC HEAT

EXCHANGE DEVICE

6. MAGNETOCALORIC HEAT EXCHANGE DEVICE

Presently the most widely recognized methods for refrigeration and cooling is utilizing gas compressors. These compressors are used with heat exchangers to bring down the temperature of the refrigerant gas and in this way cooling effect is produced. Recently, there have been studies directed on an alternate procedure that could radically lessen expenses of cooling, substituting compressors with magnetocaloric materials [63]. As a result of this, magnetic refrigeration is not extensively utilized in the United States, thus our objective of making an efficient cooling device that will lead the way towards more effective refrigeration.

In order to create a working cooling framework utilizing magnetocaloric materials, it requires a method for both turning the magnetic field on and off as well as incorporating heat exchangers with the strong magnetocaloric material (MCM). This framework will utilize water as the heat exchange liquid and Lanthanum Iron Silicon with cobalt substitution as the strong refrigerant. The device will shift back and forth between a hot and cold cycle utilizing solenoid valves and a DC motor controlled by an Arduino micro-controller. This device has the potential to diminish environmental risks associated with the disposal of Freon refrigerants in current cooling equipment, improve the efficiency of refrigeration, and be a steppingstone towards solid state refrigeration.

6.1. Current Design

The magnetocaloric effect was demonstrated again in 2002 by a group at the University of Amsterdam using MnFe alloys [64]. The first commercial magnetic cooling system was announced in 2016 by Cooltech Applications, a leading company in magnetic refrigeration [65]. The magnetic cooling system was the first commercially efficient system that is destined to be available in the refrigeration market. Despite the fact that Cooltech applications has given a solution for magnetic refrigeration, this design comes up short on the utilization of modern technology. The Cooltech magnetic refrigerator (Figure 6.1) [65] utilizes essential mechanical components, for example, fans and pumps. It has two electrically controlled continuously rotating permanent magnets.
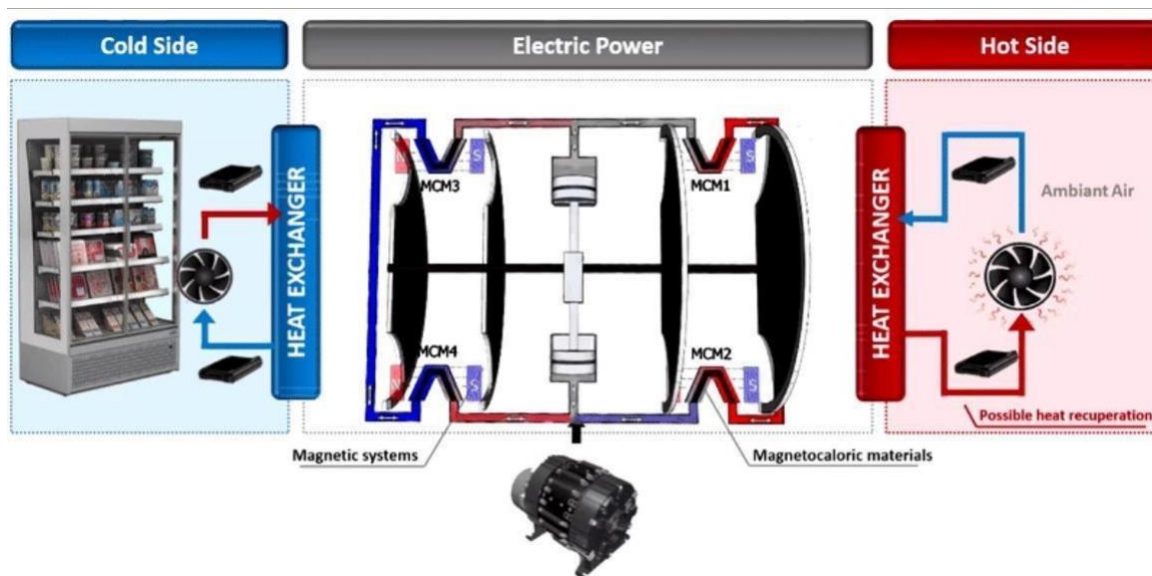
Figure 6.1: The Cooltech Refrigeration Design [65]

6.2. Proposed Design

The refrigeration system designed by Cooltech utilizes simple components, but it is a complex mechanical design for a problem that can be solved in a less complex solution that uses microcontrollers. In our proposed design, we built up the magnetic cooling device with an electronic control framework. This helped with the simplification of controlling the hot and cold-water flows in the pipes and controlling the applied magnetic fields. These flows and magnetic fields are controlled by microcontrollers that are programmed based on time. Other components of the magnetic cooling device include pumps, pipes, solenoid valves, controls and electromagnets. This design can be economical and environmentally safe as compared to traditional refrigerators. As previously mentioned more research can be done to make it more efficient by controlling solenoid valve such that even small volume of hot side water is not mixed with cold side water when the cycle is reversed. Figure 6.2 [46] represents the improved propped design.
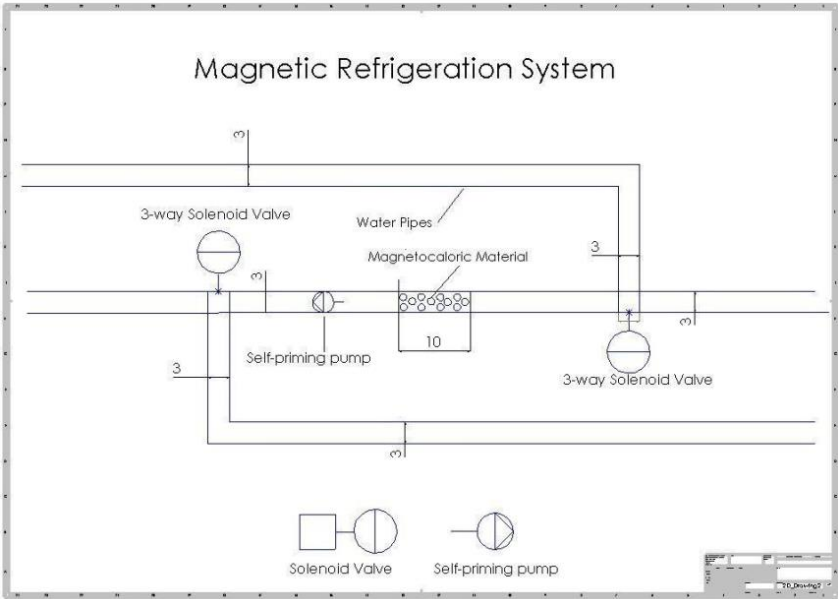
Figure 6.2: Improved Proposed Design [46]

To begin with, our design doesn't have a compressor that is used in present day refrigerator. By replacing this one component with a magnetocaloric material that utilizes pure water as the coolant liquid, any potential negative outcome because of compressor will be completely avoided. Figure 6.2 shows the new improved proposed design and annotated section 10 in Figure 6.2 is magnetocaloric holder. From Chapter 6, the change in temperature for this design will be around 4 Kelvins for non-milled sample stored in water which is specifically for prototyping a small scale magnetologic refrigeration system. To increase the surface area of every non-milled piece the holder is 3-D designed as shown in Figure 6.3 using solid works designing software and units are in length measurement units are in inches.

The linked image cannot be displayed. The file may have been moved, renamed, or deleted. Verify that the link points to the correct file and location.
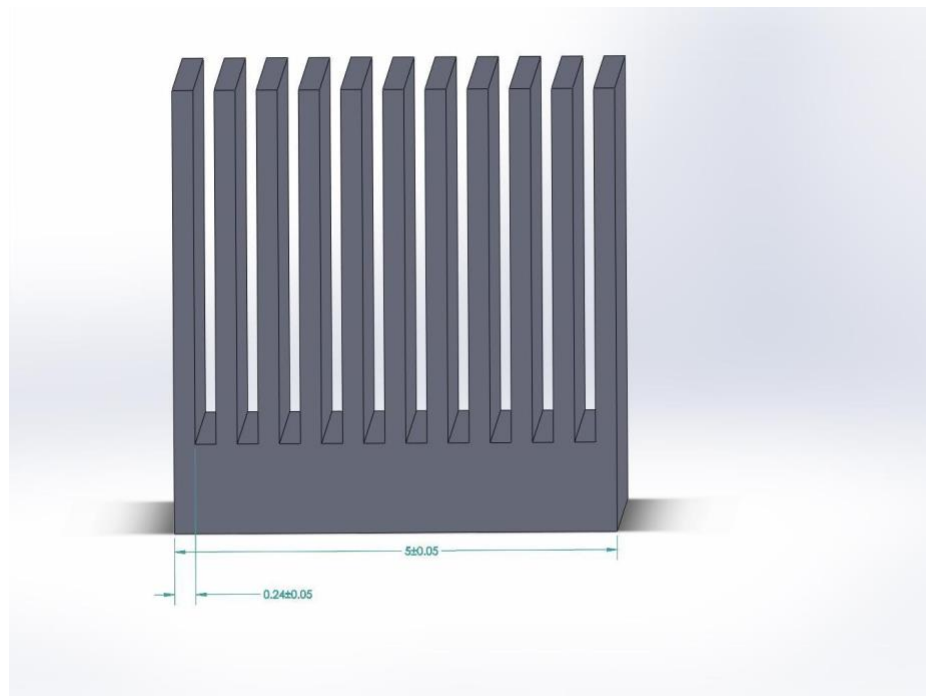
Figure 6.3: Design of Magnetocaloric Material Holder
in Magnetic Cooling Device [46]

6.3.   Design Block Diagram

This magnetic refrigeration device based on LaFe$_x$Co$_y$Si$_{13x-y}$ is ecofriendly as compared to traditional refrigerators. The amount of LaFeCoSi used for this prototype design is very low and the parts of this system are easy to replace with less size constraints. Figure 6.4 is the representation of design's block diagram. Magnetocaloric material is characterized to determine feasibility of designing the magnetic refrigeration device.
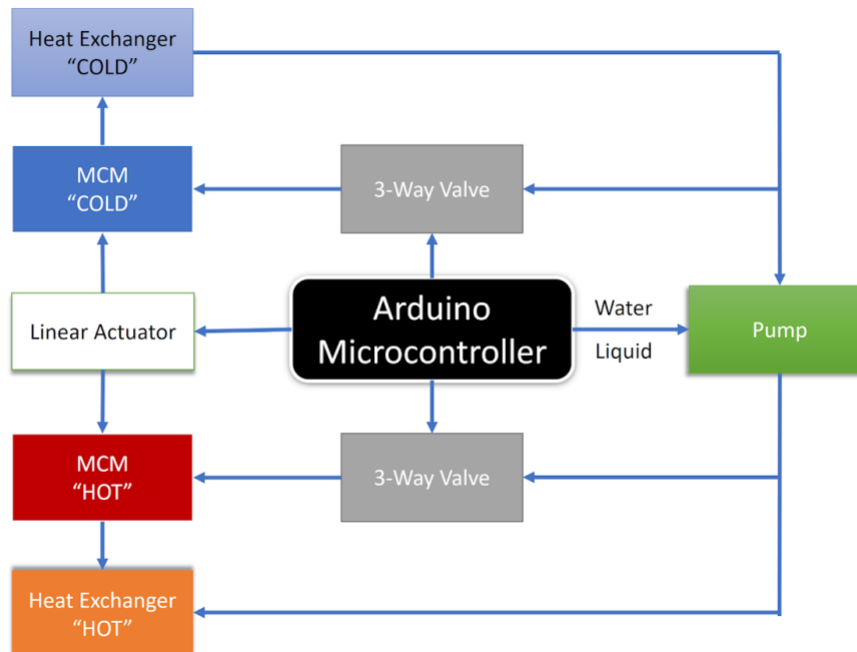
Figure 6.4: Block Diagram of the Magnetocaloric Cooling Device System [46]

CHAPTER 7

CONCLUSION AND

FUTURE WORK

7. CONCLUSION AND FUTURE WORK

7.1. Summary

Comparing the experimental results of different characterization measurements of Lanthanum Iron Silicide Cobalt, it can be easily concluded that this material exhibits giant magnetocaloric effect that can be used to design energy efficient magnetic cooling device. The main focus of this thesis research is to characterize this material and understand its properties so it can be properly utilized for designing of magnetocaloric heat exchange device. Four samples were synthesized by Ames Lab and results were compared so the best material can be selected. From the experimental measurements and analysis, it can be seen that non-milled water sample is the best choice for designing of magnetic cooling device.

Arrott plot of non-milled water sample shows that it has second order phase transition from ferromagnetic to paramagnetic phase. SEM analysis helped to understand the topography of these materials. Non milled air samples' surfaces are flat and milled air samples' surfaces are crushed into pieces while on the other hand these samples kept in water looks cloudy. X-Ray diffraction analysis of non-milled samples show $LaCo_{13}$ like structure.

Transition at 300K for all samples is a transition from ferromagnetic $La(Fe_xCo_ySi_{1-x-y})_{13}$ phase to paramagnetic $La(Fe_xCo_ySi_{1-x-y})_{13}$ phase. The water milled samples show incompletion transition and retains large magnetization even beyond 400K. This is indicative of formation of a ferromagnetic phase in the sample. Magnetization vs temperature for range of 300K to 1000K of non-milled water sample transition near 950 K inductive of formation of iron (III) oxide in the

sample. Change in entropy plays vital role in determining the magnetocaloric effect of the magnetocaloric material. Analysis of heat capacity among non-milled air and water sample demonstrate that heat capacity is increased due to addition of water in non-milled material. Change in entropy is calculated with two different methods i.e. using Maxwell's relations and heat capacity data. The result of maximum change in entropy came out to be very close to 10.5 J/Kg.K for non-milled water sample and 7 J/Kg.K for non-milled air sample from both approaches. The adiabatic temperature change of non-milled $LaFe_xCo_ySi_{13-x-y}$ stored in water and air in the temperature range from 250 K to 320 K for a magnetic field change from 0 to 3 Tesla shows that temperature change is greatest in non-milled sample stored in water i.e. 3.67 Kelvins as compared to the one stored in air i.e. 2.76 Kelvins.

This analysis demonstrates that the change in temperature and entropy of $La(Fe_xCo_ySi_{1-x-y})_{13}$ is increased when it is stored in water and as result, it makes it a better choice for magnetic refrigeration device. The improved proposed design of magnetocaloric heat exchange device is designed such that the magnetocaloric material holder has perforated channels to increase the water contact with the material.

7.2. Future Work

Future work can be done to improve the design of magnetocaloric heat exchange device. This research analysis can be utilized to design the device effectively. Magnetocaloric material holder can be redesigned to maximize the contact of water and avoid the deterioration of material in water as Lanthanum Iron Silicide Cobalt tend to deteriorate when kept in water for long time. Variety of coatings on the material can be tried to avoid this deterioration while making sure these coatings don't affect the magnetocaloric properties of the material.

Instead of 3-way valve 2-way valves can be used so that system can be controlled and programmed conveniently. Also, more research can be done to thoroughly analyze the time cycle to better understand its effect on efficiency of cold cycle and the cooling effect of the device can be maximized. The fluid flow, head pump velocity, pressure of flowing water and other factors can optimize to maximize the cooling affect. Fluid systems and modern approaches such as EES can be used to optimize the fluid flow factor. Opening and closing of both hot and cold cycle can be controlled by installation of thermometer in the water. Arduino controlled pumps and addition of secondary water cycles can optimize the design, the learning curve for the magnetocaloric heat exchange device is big.

Reference

[1]   "Parkinson, Desmond John, (8 March 1913–20 May 1996), Under-Secretary, Agricultural Research Council, 1971–73," in *Who Was Who*, Oxford University Press, 2007.

[2]   C. Gurdgiev, "Summary of Comments on the European Commission Green Paper 'Building a Capital Markets Union,'" *SSRN Electron. J.*, 2015, doi: 10.2139/ssrn.2592918.

[3]   R. Zogg, W. Goetzler, C. Ahlfeldt, H. Hiraiwa, A. Sathe, and T. Sutherland, "Energy Savings Potential and Research, Development, & Demonstration Opportunities for Commercial Building Appliances," Office of Scientific and Technical Information (OSTI), 2009. doi: 10.2172/1219984.

[4]   G. J. M. Velders, D. W. Fahey, J. S. Daniel, M. McFarland, and S. O. Andersen, "The large contribution of projected HFC emissions to future climate forcing," *Proc. Natl. Acad. Sci. U. S. A.*, vol. 106, no. 27, pp. 10949–10954, Jul. 2009, doi: 10.1073/pnas.0902817106.

[5]   "Application of Best Industry Practices to the Design of Commercial Refrigerators," Office of Scientific and Technical Information (OSTI), 2002. doi: 10.2172/907887.

[6]   P. Weiss and A. Piccard, "Le phénomène magnétocalorique," *J. Phys. Théorique Appliquée*, vol. 7, no. 1, pp. 103–109, 1917, doi: 10.1051/jphystap:019170070010300.

[7]   E. Warburg, "Magnetische Untersuchungen," *Ann. Phys.*, vol. 249, no. 5, pp. 141–164, 1881, doi: 10.1002/andp.18812490510.

[8]   J. E. Zimmerman, D. B. Sullivan, and S. E. McCarthy, "Refrigeration for cryogenic sensors and electronic systems," National Bureau of Standards, 1981. doi: 10.6028/nbs.sp.607.

[9] V. K. Pecharsky and K. A. Gschneidner Jr, "Magnetocaloric effect and magnetic refrigeration," *J. Magn. Magn. Mater.*, vol. 200, no. 1–3, pp. 44–56, 1999, doi: 10.1016/s0304-8853(99)00397-2.

[10] J. Sun, W. Li, and B. Cui, "Energy and exergy analyses of R513a as a R134a drop-in replacement in a vapor compression refrigeration system," *Int. J. Refrig.*, vol. 112, pp. 348–356, 2020, doi: 10.1016/j.ijrefrig.2019.12.014.

[11] "An Ice Cold Epic: The History of Commercial Refrigerators," *Imbera FoodService*, 2015. .

[12] D. R. Brown, J. A. Dirks, N. Fernandez, and T. E. Stout, "The Prospects of Alternatives to Vapor Compression Technology for Space Cooling and Food Refrigeration Applications," Office of Scientific and Technical Information (OSTI), 2010. doi: 10.2172/979500.

[13] "Magnetic refrigeration," *Physics Subject Headings (PhySH)*. American Physical Society (APS), doi: 10.29172/391d8598-aef3-4799-9fdb-fc950d2a6fc4.

[14] Z. Gang and L. Qing, "Realization of the cooperation between traveling wave component and standing wave component in thermoacoustic regenerator." AIP Publishing LLC, 2014, doi: 10.1063/1.4860754.

[15] D. R. Brown, T. B. Stout, J. A. Dirks, and N. Fernandez, "The Prospects of Alternatives to Vapor Compression Technology for Space Cooling and Food Refrigeration Applications," *Energy Eng.*, vol. 109, no. 6, pp. 7–20, 2012, doi: 10.1080/01998595.2012.10554226.

[16] T. Christiaanse and E. Brück, "Proof-of-Concept Static Thermomagnetic Generator

Experimental Device," *Metall. Mater. Trans. E*, vol. 1, no. 1, pp. 36–40, 2014, doi: 10.1007/s40553-014-0006-9.

[17] E. L. T. França, A. O. dos Santos, A. A. Coelho, and L. M. da Silva, "Magnetocaloric effect of the ternary Dy, Ho and Er platinum gallides," *J. Magn. Magn. Mater.*, vol. 401, pp. 1088–1092, Mar. 2016, doi: 10.1016/j.jmmm.2015.10.138.

[18] V. Franco, J. S. Blázquez, B. Ingale, and A. Conde, "The Magnetocaloric Effect and Magnetic Refrigeration Near Room Temperature: Materials and Models," *Annu. Rev. Mater. Res.*, vol. 42, no. 1, pp. 305–342, Aug. 2012, doi: 10.1146/annurev-matsci-062910-100356.

[19] W. F. Giauque, "A THERMODYNAMIC TREATMENT OF CERTAIN MAGNETIC EFFECTS. A PROPOSED METHOD OF PRODUCING TEMPERATURES CONSIDERABLY BELOW ABSOLUTE," *J. Am. Chem. Soc.*, vol. 49, no. 8, pp. 1864–1870, Aug. 1927, doi: 10.1021/ja01407a003.

[20] W. F. Giauque and D. P. MacDougall, "Attainment of Temperatures Below 1{\textdegree} Absolute by Demagnetization {ofGd}2({SO}4)3$\cdotp$8H2O," *Phys. Rev.*, vol. 43, no. 9, p. 768, May 1933, doi: 10.1103/physrev.43.768.

[21] J. A. Barclay, "Refrigeration for Cryogenic Sensors," in *Second Biennial Conference on Refrigration for Cryogenic Sensors and Electronic System*, 1983.

[22] C. Aprea, A. Greco, A. Maiorino, and C. Masselli, "Analyzing the energetic performances of {AMR} regenerator working with different magnetocaloric materials: Investigations and viewpoints," *Int. J. Heat Technol.*, vol. 35, no. Special Issue1, pp. S383--S390, Sep. 2017,

doi: 10.18280/ijht.35sp0152.

[23] C. Zimm *et al.*, "Description and Performance of a Near-Room Temperature Magnetic Refrigerator," in *Advances in Cryogenic Engineering*, Springer {US}, 1998, pp. 1759–1766.

[24] O. Cell and C. Change, "Ozone layer protection," *Ozone layer Prot.*, vol. 5, no. 128, 1995, doi: 10.1596/0-8213-3133-7.

[25] E. Brück, H. Yibole, and L. Zhang, "A universal metric for ferroic energy materials," *Philos. Trans. R. Soc. A Math. Phys. Eng. Sci.*, vol. 374, no. 2074, p. 20150303, Aug. 2016, doi: 10.1098/rsta.2015.0303.

[26] "Debut for magnetic refrigeration wine cooler," *Capital Web Ltd*, 06-Jan-2015.

[27] BASF, "Premiere of cutting-edge magnetocaloric cooling appliance," *YouTube*, 2015. https://www.youtube.com/watch?feature=player_embedded&v=jnl9m0rSE7U&x-yt-ts=1421914688&x-yt-cl=84503534 (accessed Apr. 02, 2020).

[28] A. Gaved, "First Magnetic Refrigeration System for Commercial Refrigeration Launches," *BNP Media*, 20-Jun-2016.

[29] L. Wood, "Magnetic Refrigeration Market to Reach $163 Million by 2023: Analysis By Product & Application," *Cision PR Newswire*, Dublin, 27-Jul-2017.

[30] U. S. E. P. Agency, "HCFCs and the Ozone Layer Phasing Out HCFC Refrigerants To Protect The Ozone Layer Phaseout of R-22 and R142b Availability and Cost of R-22 Buying a New Air Conditioner Servicing Systems with R-22," 2020.

[31]   H. Griffiths, "Spike in banned ozone-eating CFC gases linked to China in new research," *CNN*, Hong Kong, 2019.

[32]   "Is Magnetic Refrigeration the Future of Commercial Refrigeration?," *Sensigreen Mechanical*. .

[33]   A. Subramaniam, "Vacuum Arc Melting Unit," *http://home.iitk.ac.in/~anandh/lab/Arc_Melting.pdf*, no. i, p. 2, [Online]. Available: http://home.iitk.ac.in/~anandh/lab/Arc_Melting.pdf.

[34]   J. D. Verhoeven, *Fundamentals of Physical Metallurgy*. Wiley, 1975.

[35]   K. Wright, "The Origins and development of ground stone assemblages in Late Pleistocene Southwest Asia," *Paléorient*, vol. 17, no. 1, pp. 19–45, 1991, doi: 10.3406/paleo.1991.4537.

[36]   "8000D Mixer/Mill® - Dual High-Energy Ball Mill," *SPEXSamplePrep*. .

[37]   M. Carter and J. Shieh, "Microscopy," in *Guide to Research Techniques in Neuroscience*, Elsevier, 2015, pp. 117–144.

[38]   "Powder Diffraction," in *X-Ray Diffraction for Materials Research*, Apple Academic Press, 2016, pp. 249–274.

[39]   A. Chodos, "New Prototype Magnetic Refrigerators Hold Commercial Promise," *APS Phys.*, vol. 12, 2003.

[40]   J. Lyubina, "Magnetocaloric Materials," *Novel Functional Magnetic Materials*. Springer International Publishing, pp. 115–186, 2016, doi: 10.1007/978-3-319-26106-5_4.

[41] D. T. Cam Thanh *et al.*, "Structure, magnetism, and magnetocaloric properties of MnFeP1−xSix compounds," *J. Appl. Phys.*, vol. 103, no. 7, p. 07B318, 2008, doi: 10.1063/1.2836958.

[42] G. Barbezat and H. Mayer, "Les fontes à graphite sphéroïdal de structure bainito-austénitique," *Matériaux Tech.*, vol. 75, no. 9, pp. 364–370, 1987, doi: 10.1051/mattech/198775090364.

[43] J. Steven Brown and P. A. Domanski, "Review of alternative cooling technologies," *Appl. Therm. Eng.*, vol. 64, no. 1–2, pp. 252–262, 2014, doi: 10.1016/j.applthermaleng.2013.12.014.

[44] J.-S. Fang, M.-R. Jian, T.-S. Chin, H.-W. Zhang, and B.-G. Shen, "Magnetic Viscosity of NdFe11TiNxThin Films," *Jpn. J. Appl. Phys.*, vol. 39, no. S1, p. 496, 2000, doi: 10.7567/jjaps.39s1.496.

[45] B. G. Shen, J. R. Sun, F. X. Hu, H. W. Zhang, and Z. H. Cheng, "Recent Progress in Exploring Magnetocaloric Materials," *Adv. Mater.*, vol. 21, no. 45, pp. 4545–4564, 2009, doi: 10.1002/adma.200901072.

[46] Y. Javed, K., Garcia, H., Hutton, M., Nguyen, Q., & Maly, "Magnetic Cooling Device: A Path Towards Energy Efficient Refrigeration," 16/394,688, 2018.

[47] C. R. S. Tool, "VersaLab Free Disign Quantum," *Trans. ASME J. Appl. Mech.*, no. October, pp. 1–47, 2006, doi: 10.13155/29825.

[48] Quantum Design, "Physical Property Measurement System, DynaCool User's Manual," no.

1307, 2011.

[49] E.A. Skrabek and W.E. Wallace, "Magnetic Characteristics of Laves Phases Containing Lanthanide Metals Combined with Nickel," *AIP J. Appl. Phys.*, 2004, doi: 10.1063/1.1729507.

[50] J. E. Greedan, "Magnetic Oxides," in *Encyclopedia of Inorganic and Bioinorganic Chemistry*, John Wiley & Sons, Ltd, 2011.

[51] V. Franco, J. S. Blázquez, J. J. Ipus, J. Y. Law, L. M. Moreno-Ramírez, and A. Conde, "Magnetocaloric effect: From materials research to refrigeration devices," *Prog. Mater. Sci.*, vol. 93, pp. 112–232, 2018, doi: 10.1016/j.pmatsci.2017.10.005.

[52] O. Gutfleisch, A. Yan, and K.-H. Müller, "Large magnetocaloric effect in melt-spun LaFe13−xSix," *J. Appl. Phys.*, vol. 97, no. 10, p. 10M305, 2005, doi: 10.1063/1.1847871.

[53] J. Liu *et al.*, "Exploring La(Fe,Si)13-based magnetic refrigerants towards application," *Scr. Mater.*, vol. 67, no. 6, pp. 584–589, 2012, doi: 10.1016/j.scriptamat.2012.05.039.

[54] M. F. J. Boeije, M. Maschek, X. F. Miao, N. V Thang, N. H. van Dijk, and E. Brück, "Mixed magnetism in magnetocaloric materials with first-order and second-order magnetoelastic transitions," *J. Phys. D. Appl. Phys.*, vol. 50, no. 17, p. 174002, 2017, doi: 10.1088/1361-6463/aa5db9.

[55] A. H. Morrish, *The Physical Principles of Magnetism*. IEEE, 2001.

[56] J. S. Lee, "Evaluation of the magnetocaloric effect from magnetization and heat capacity data," *Phys. status solidi*, vol. 241, no. 7, pp. 1765–1768, Jun. 2004, doi:

10.1002/pssb.200304685.

[57] A. Fujita, S. Fujieda, Y. Hasegawa, and K. Fukamichi, "Itinerant-electron metamagnetic transition and large magnetocaloric effects {inLa}({FexSi}1-x)13compounds and their hydrides," *Phys. Rev. B*, vol. 67, no. 10, Mar. 2003, doi: 10.1103/physrevb.67.104416.

[58] T. Gottschall *et al.*, "Making a Cool Choice: The Materials Library of Magnetic Refrigeration," *Adv. Energy Mater.*, vol. 9, no. 34, p. 1901322, Jul. 2019, doi: 10.1002/aenm.201901322.

[59] R. Hadimani, "Advanced Magnetoelastic and Magnetocaloric Materials for Device Applications," Cardiff University, 2009.

[60] G. Wang and I. E. First-order, "Magnetic and Calorimetric Study of Magnetocaloric Effect in Inter-Metallics Exhibiting First Order Magnetostructural Transitions," 2012.

[61] M. I. Ilyn, A. M. Tishin, K. A. Gschneidner, V. K. Pecharsky, and A. O. Pecharsky, "Magnetothermal Properties of Polycrystalline Gd2In," in *Cryocoolers 11*, Springer {US}, 2002, pp. 457–464.

[62] C. A. Swenson, "Erratum: Linear thermal expansivity (1.5{\textendash}300 K) and heat capacity (1.2{\textendash}90 K) of Stycast 2850FT [Rev. Sci. Instrum. 68, 1312 (1997)]," *Rev. Sci. Instrum.*, vol. 68, no. 6, p. 2596, Jun. 1997, doi: 10.1063/1.1148453.

[63] J. Kagathara, S. Wieland, E. Gärtner, V. Uhlenwinkel, and M. Steinbacher, "Heat Treatment and Formation of Magnetocaloric 1:13 Phase in {LaFe}11.4Si1.2Co0.4 Processed by Laser Beam Melting," *Materials (Basel).*, vol. 13, no. 3, p. 773, Feb. 2020, doi:

10.3390/ma13030773.

[64] S. C. Madireddi, "Role of extrinsic factors in utilizing the Giant Magnetocaloric Effect on materials: Frequency and time dependence," Iowa State University.

[65] "Cooltech's Magnetic Refrigeration System," *CoolTech Applications*.

Stability of magnetocaloric La(Fe$_x$Co$_y$Si$_{1-x-y}$)$_{13}$ in water and air

Khushar Javed (iD), Shalabh Gupta, Vitalij K. Pecharsky, and Ravi L. Hadimani (iD)

COLLECTIONS

Paper published as part of the special topic on 2019 Joint MMM-Intermag Conference

View Online   Export Citation   CrossMark

ARTICLES YOU MAY BE INTERESTED IN

Stability of magnetocaloric La(Fe$_x$Co$_y$Si$_{1-x-y}$)$_{13}$ in water and air

Khushar Javed,[1,a] (ID)Shalabh Gupta,[2] Vitalij K. Pecharsky,[2,3] and Ravi L. Hadimani[1,4,a] (ID)

AFFILIATIONS

[1] Department of Mechanical and Nuclear Engineering, Virginia Commonwealth University, Richmond, Virginia 23284, USA
[2] Division of Materials Science and Engineering, Ames Laboratory, US Department of Energy, Ames, Iowa 50011, USA
[3] Department of Materials Science and Engineering, Iowa State University, Ames, Iowa 50011, USA
[4] Department of Biomedical Engineering, Virginia Commonwealth University, Richmond, Virginia 23284, USA

Note: **This paper was presented at the 2019 Joint MMM-Intermag Conference.**
[a] Email: javedk@vcu.edu **and** rhadimani@vcu.edu

ABSTRACT

Stability of cobalt-doped lanthanum iron silicide, La(Fe$_x$Co$_y$Si$_{1-x-y}$)$_{13}$ have been investigated under conditions required for magnetocaloric refrigeration. The XRD analysis revealed that both milled and non-milled samples stored in water loose a few Bragg peaks corresponding to the NaZn$_{13}$ phase of La(Fe$_x$Co$_y$Si$_{1-x-y}$)$_{13}$. Samples stored in air show well-defined Bragg peaks similar to that of pristine material. The SEM-EDS of the milled and non-milled samples stored in water and air show an increased concentration of oxygen in the samples, particularly those treated with water. The course non-milled powders stored in air and water show sharp transitions at the Curie temperature T$_C$ = 300K without large magnetization above the T$_C$. The milled, fine-particulate sample stored in air shows a slightly broadened transition at T$_C$, and that stored in deionized water for 14 days shows significantly broadened transition from 300K and retains large magnetizations above 400 K. This is indicative of relatively fast hydrolysis and removal of some or all of La, likely as hydroxide, from fine powders, leaving behind La-poor or, potentially, La-free Fe-Co-Si containing ferromagnetic residue with much higher Curie temperature. The non-milled course sample stored in water has sharper magnetic transition and higher magnetization hence it shows the highest entropy change among all 4 type of samples.

INTRODUCTION

Magnetocaloric refrigeration is an upcoming environmentally friendly cooling method which is based on magnetocaloric effect observed in ferromagnetic materials. In addition to its high efficiency, this promising cooling technology is an attractive alternative to vapor compression systems that employ harmful CFC and HCFC as working fluids.[1] The cooling efficiency in magnetic refrigerators is higher (the magnetic cooling efficiency can be reached up to 60% of a Carnot cycle, whereas it is only 5–10% for vapor compression refrigeration) even at a small scale, enabling the development of portable, battery-powered products.[2] Giant magnetocaloric effects are observed in materials that undergo a first-order magnetic transition (FOMT), because the FOMT is associated with an abrupt change in crystallographic lattice which enhances magnetocaloric effects (MCE) via a spin–lattice coupling.[3,4] Pecharsky et. al reported

'Giant Magnetocaloric Effect' in Gd$_5$Si$_2$Ge$_2$ near room temperature,[3,4] an event that sparked worldwide interest in developing new kinds of magnetocaloric materials and magnetic refrigeration systems. The first order phase transition materials also exhibit other extreme properties such as giant magnetoresistance and colossal magnetostriction at the phase transition temperature which can be used in many sensor and actuator applications.[5–7] Lanthanum iron Silicon with cobalt substitution is a potential magnetocaloric material that can be used in commercial magnetocaloric refrigerators due its low materials cost and comparable adiabatic temperature change upon application of magnetic field.[8–10]

In this paper, we have investigated the stability of coarsely ground (non-milled) particles and milled fine particles under different conditions that are needed for optimal operation of magnetic refrigerator. Four different types of La(Fe$_{0.842}$Co$_{0.073}$Si$_{0.084}$)$_{13}$ particles are characterized. These include two milled fine particle
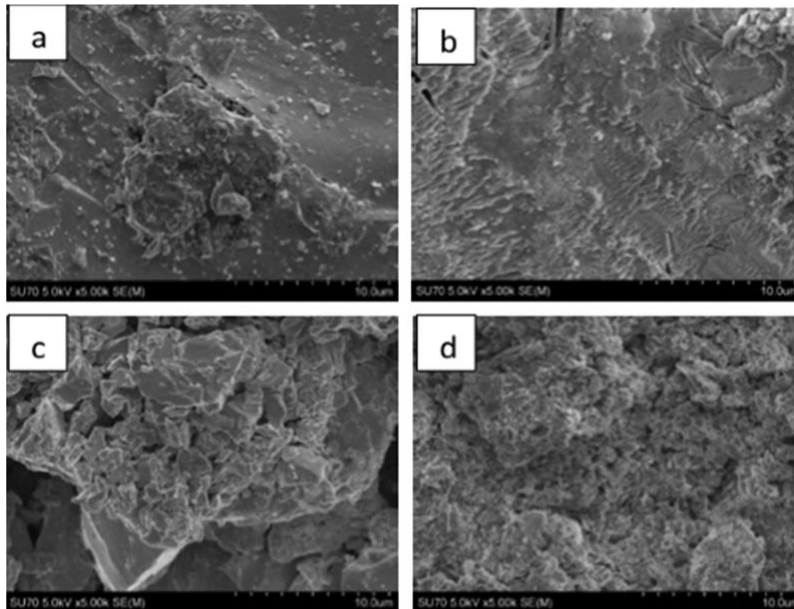
FIG. 1. SEM analysis of LaFeSiCo (a) Non-milled sam- ple stored in air (b) Non-milled sample stored in deoinized stored in water (c) Milled sample stored in air (d) Milled sample stored in deionized water for 14 days.

samples, one placed in air and water, similarly the other 2 non-milled samples placed in air and water. The coarse non-milled samples have particle size of about 50-100 microns and fine milled samples have particle size below 1 micron. These samples are character- ized by comparison of XRD analysis, SEM, elemental composition, magnetization vs. temperature, magnetization vs. magnetic field and change in entropy vs. temperature for a magnetic field change of 5T. The non-milled coarse samples exhibit better magnetocaloric effect (MCE) when stored in water as compared to the one stored in air.

EXPERIMENTAL DETAILS

Preparation of bulk La(Fe$_x$Co$_y$Si$_{1-x-y}$)$_{13}$

The sample with a nominal composition of La(Fe$_{0.842}$Co$_{0.073}$Si$_{0.084}$)$_{13}$ was prepared by arc-melting of elements under argon atmosphere. A total of 20 g of elements, taken in stoichiometric pro- portions, were melted together on a water-cooled Cu-hearth. The ingot was then re-melted four times and was turned over each time to achieve homogeneity. The total measured weight loss was less than 0.5 wt. %. The as-cast ingot was broken into smaller pieces, which were then wrapped within a tantalum-foil and sealed inside fused-silica tube under vacuum for further heat treatment. The Ingot pieces were annealed at 1050° C for one week followed by quenching in ice-cold water.

Ball milling to obtain submicron particles

To obtain the milled sample, the annealed pieces were crushed in an agate mortar inside an argon-filled glove box and sieved to a uniform particle size of 100μ or below. This powder was then ball-milled in hardened steel containers using a SPEX8000 mill. Milling was performed for 10 mins. in argon atmosphere and under dry conditions using a ball-to-powder ratio of approximately 1:1.

After milling, powder was removed from the containers and used

TABLE I. EDS analysis of La(Fe$_{0.842}$Co$_{0.073}$Si$_{0.084}$)$_{13}$ (a) Non-milled sample stored in air (b) Non-milled sample stored in deoinized water for 14 days (c) Milled sample stored in air (d) Milled sample stored in deionized water for 14 days.

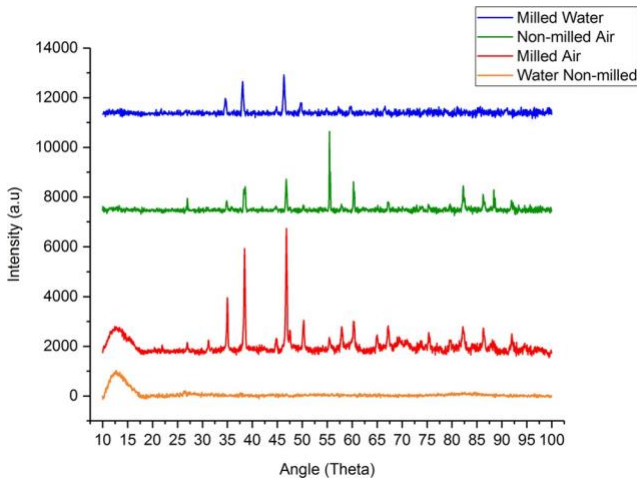| Elements	Wt%	At%
(a)		
OK	1.7	6.2
SiK	3.15	6.6
LaL	19.8	8.4
FeK	69.6	73
CoK	5.81	5.8
(b)		
OK	5.58	19.2
SiK	3.38	6.27
LaL	17.6	6.6
FeK	68.28	63.7
CoK	4.86	4.3
(c)		
OK	3.28	12
SiK	2.51	5.1
LaL	19.4	7.9
FeK	69	70
CoK	7.5	5.6
(d)		
OK	8.59	26.7
SiK	2.6	4.61
LaL	18.97	6.8
FeK	62.33	55.5
CoK	7.5	6.33

FIG. 2. X-Ray diffraction patterns of milled and non-milled La(Fe$_x$Co$_y$Si$_{1-x-y}$)$_{13}$ samples stored in water and air recorded using Cu Kα radiation.

for characterization and magnetic measurements. Similar milling process has been used and reported for other rare-earth magnetic nanoparticles by us.[11]

RESULTS

SEM and EDS analysis

Figures 1 is obtained utilizing Ultra High-Resolution Analytical FE-SEM SU-70 at the secondary electron image resolution of 5k at 5 kV. Figure 1 shows the SEM analysis of the samples. As it can be clearly seen in the Figure 1(d) more water is absorbed by milled sample as compared to the nonmilled sample stored in water. Milling increased the surface area and as a result milled sample had smaller particle allowing more water to react efficiently as com- pared to nonmilled sample particles. Table I presents the elemental composition of all four samples. Milled sample stored in air has the

maximum amount of Oxygen that is from the contamination of the water.

XRD analysis

PANalytical X'PertPro diffractometer is used to determine crystal structure of the samples. Samples began to lose peaks when contaminated with water as shown in Fig. 2. Based on this X-Ray diffraction samples air Non-Milled sample show LaCo$_{13}$ like struc- ture but the lattice parameters are larger than LaCo$_{13}$ compound. There is a huge peak at 55 deg which may arise from preferred ori- entation or an impurity that is susceptible to decomposition in air. Water Non-Milled sample show LaCo$_{13}$ like structure but the lat- tice parameters are larger than LaCo$_{13}$ compound. Except for the 55-degree peak rest of the pattern appears to be more or less similar to as-synthesized material.

Magnetic measurements

Figure 3 presents the relationship between magnetization (emu/g) and temperature (K) at an applied magnetic field of 0.01T. Both milled samples stored in air and water have broader transi- tion temperatures around 300 K whereas, both non-milled samples stored in air and water have sharp transitions at 300 K. Milled sam- ple that is stored in water has highest magnetization and retains large magnetization above 300 K. This is indicative of relatively fast hydrolysis and removal of some or all La as hydroxide from fine powders, leaving behind La-poor or, potentially, La-free Fe- Co-Si containing ferromagnetic residue with much higher Curie temperature.

Figure 3(a) shows magnetization vs. magnetic field at 300K. Milled sample that is stored in water shows the highest satura- tion magnetization followed by both non-milled samples and milled sample stored in air. Non-milled sample stored in water has the highest relative permeability. Addition of water to both milled and non-milled samples increase magnetization compared to the samples stored in air as seen in Figure 3.

Entropy is one of the main parameters to characterize any mag- netocaloric material. Based on the M-H curves, the magnetic entropy
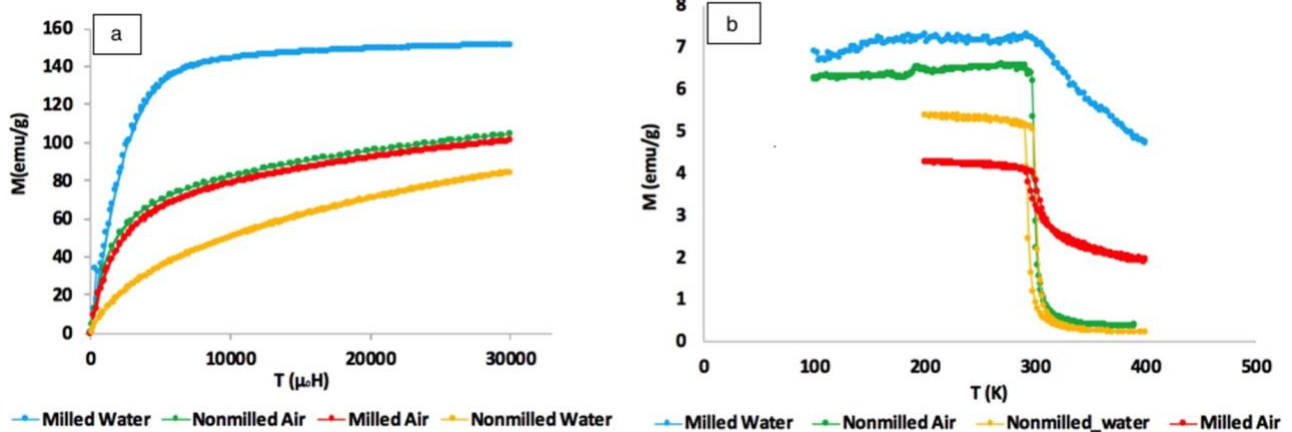

FIG. 3. Magnetic measurements of La(Fe$_x$Co$_y$Si$_{1-x-y}$)$_{13}$ samples (a) Magnetization (emu/g) vs. Magnetic Field (T) at 300 K (b) Magnetization (emu/g) vs. Temperature (K) at 0.01 T.

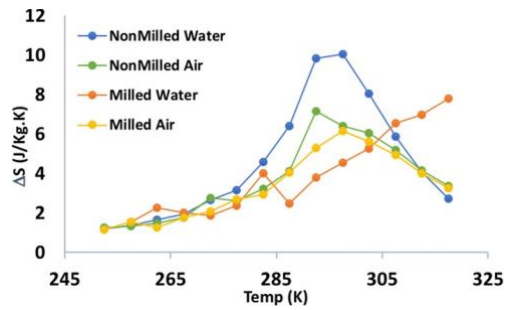**FIG. 4**. δS vs. Temperature for a magnetic field change of 3T.

change can be calculated using the Maxwell's equation.[3]

$$\delta S = \int_o^H \mu 0\left(\frac{\partial M}{\partial T}\right)dH$$

Fig. 4 shows the temperature dependence of the change in magnetic entropy for the characterized samples for a magnetic field change of 3T. The change in entropy is highest closer to the magnetic transition temperature like other magnetocaloric materials where ferromagnetic to paramagnetic phase transitions will show the maximum entropy change.[4]

The curve of the non-milled sample store in water shows the maximum change in magnetic entropy value of 11 J $Kg^{-1}K^{-1}$ near 300 K while the milled sample stored in water has the lowest entropy change. Maximum magnetic entropy change of ΔS_M (T, H) as function of temperature of $LaFe_{11.6-x} Co_x Si_{1.4}$ compounds (x = 0.5) has maximum entropy of 7.5 J/Kg.[12] LaFeSiCo milled and nonmilled sample stored in air shows almost same delta S except around 292 K. As shown in Fig. 3(a) Magnetization vs. Magnetic Field of milled and nonmilled sample stored in air shows similar curve at 300 K that can also be seen from the Fig. 4 change in entropy of these two samples at 300 K is almost equivalent.

DISCUSSION

Milling process has significantly broadened the transition hence milled sample stored in water has the lowest entropy change. Magnetic refrigerator is a complex structure that includes fabrication of magneto-caloric material bed. This process requires the formulation of powder of MCM. This magnetocaloric bed when in contact with water might oxidize the material. Addition of water to both milled and non-milled samples has increased the magnetization which may be due to formation of Fe_3O_4. The increase in magnetization in water stored sample has resulted in higher entropy change. In a magnetic cooling device water can be used in as a heat transfer fluid for efficient transfer of heat from the magnetocaloric material to the heat exchanger.

CONCLUSIONS

It can be concluded that the course non-milled samples con- tain larger particles and resulted in sharper transition. Water added to the milled sample leads to hydrolysis and removal of some of the La as hydroxide from fine powders, leaving behind La-poor Fe-Co- Si containing ferromagnetic residue of possibly Fe_3O_4 or $CoFe_2O_4$

with much higher Curie temperature as follows from the absence of the large magnetization beyond 300K. The course non-milled particles show much greater stability and sharper magnetic transition when stored both in air and water. The course crushed sample stored in water has sharper magnetic transition and higher magnetization hence it shows the highest entropy change among all 4 types of samples.

Addition of water to the cobalt doped Lanthanum Iron Silicon has increased the magnetization which has resulted in the enhanced entropy change in the non-milled sample. Whereas milling process has reduced the entropy change due to broadened transition temperature and reduced magnetization compared to non-milled samples in e $La(Fe_{0.842}Co_{0.073}Si_{0.084})_{13}$ system.

REFERENCES

[1] C. Zimm, A. Jastrab, A. Sternberg, V. K. Pecharsky, K. Gschneidner, Jr., M. Osborne, and I. Anderson, "Description and performance of a near-room temperature magnetic refrigerator," Adv. Cryog. Eng. **43**, 1759–1766 (1998).

[2] M.-H. Phan and Y. Seong-Cho, "Review of the magnetocaloric effect in manganite materials," Journal of Magnetism and Magnetic Materials **308**(2), 325–340 (2007).

[3] V. K. Pecharsky and K. A. Gschneider, Jr., "Tunable magnetic regenerator alloys with a giant magnetocaloric effect for magnetic refrigeration from ~20 to~290 K," Appl. Phys. Lett. **70**(24), 3299–3301 (1997).

[4] V. K. Pecharsky and K. A. Gschneider, Jr., "Giant magnetocaloric effect in $Gd_5(Si_2Ge_2)$," Phys. Rev. Lett. **78**(23), 4494–4497 (1997).

[5] R. L. Hadimani, P. A. Bartlett, Y. Melikhov, J. E. Snyder, and D. C. Jiles, "Field and temperature induced colossal strain in $Gd_5(Si_xGe_{1-x})_4$," J. Magn. Magn. Mater. **323**(5), 532–534 (2011).

[6] R. L. Hadimani, Y. Melikhov, J. E. Snyder, and D. C. Jiles, "Anomalous behavior in electrical transport properties in single-crystal $Gd_5Si_{1.8}Ge_{2.2}$ and Polycrystalline $Gd_5Si_{2.09}Ge_{1.91}$," IEEE Trans. Magn. **45**(10), 4368–4371 (2009).

[7] R. L. Hadimani and D. C. Jiles, "Irrecoverable and recoverable resistivity resulting from the first order magnetic-structural phase transition in $Gd_5(Si_xGe_{1-x})_4$," IEEE Magn. Lett. **1**, 6000104 (2010).

[8] L. Mañosa, D. González-Alonso, A. Planes, M. Barrio, J.-L. Tamarit, I. S. Titov, M. Acet, A. Bhattacharyya, and S. Majumdar, "Inverse barocaloric effect in the giant magnetocaloric La-Fe-Si-Co compound," Nat. Commun. **2**, 595 (2011).

[9] Y. Shao, J. Liu, M. Zhang, A. Yan, K. P. Skokov, D. Y. Karpenkov, and O. Gutfleisch, "High-performance solid-state cooling materials: Balancing magnetocaloric and non-magnetic properties in dual phase La-Fe-Si," Acta Mater. **125**, 506–512 (2017).

[10] O. Gutfleisch, M. A. Willard, E. Brück, C. H. Chen, S. G. Sankar, and J. P. Liu, "Magnetic materials and devices for the 21st century: Stronger, lighter, and more energy efficient," Adv. Mater. **23**(7), 821–842 (2011).

[11] R. L. Hadimani, S. Gupta, S. Harstad, V. Pecharsky, and D. Jiles, "Investigation of room temperature ferromagnetic nanoparticles of Gd_5Si_4," IEEE Trans. Magn. **99**, 2504104 (2015).

[12] X. Chen, Y. Chen, and Y. Tang, "Phase relation of $LaFe_{11.6}Si_{1.4}$ compounds at different high-temperature and the magnetic property of $LaFe_{11.6-x}Co_x Si_{1.4}$ compounds," Bull. Mater. Sci. **35**(2), 175–182 (2012).